[AMERICAN JOURNAL OF SCIENCE, VOL. 294, DECEMBER, 1994, P. 1229–1289]

$CaO + MgO + Al_2O_3 + SiO_2 + H_2O$ TO 35 KB: AMPHIBOLE, TALC, AND ZOISITE DEHYDRATION AND MELTING REACTIONS IN THE SILICA-EXCESS PART OF THE SYSTEM AND THEIR POSSIBLE SIGNIFICANCE IN SUBDUCTION ZONES, AMPHIBOLITE MELTING, AND MAGMA FRACTIONATION

ALAN BRUCE THOMPSON* and DAVID J. ELLIS**

ABSTRACT. (Dehydration) melting of amphibolite has been proposed as a source for I-type granites and several other types of magmatic rocks. Experiments in CMASH and natural plagioclase-bearing amphibolites have shown that the fluid-absent solidus lies at temperatures of 850° to 900°C from about 2 to 12 kb. These temperatures are not easily achieved in continental collision zones. Thus, if plagioclase amphibolites are the likely source for such magmatic rocks, then they must be produced after continental collision with basalt input into the thickened crust or beneath magmatic arcs, or in environments of lithosphere heating during extension and with basalt addition, or be related to subduction zones with specific thermal parameters.

Hydrous minerals other than amphibole are stable in basaltic compositions. In CMASH zoisite and talc are stable at temperatures higher than the H_2O-saturated solidus. While the model system CMASH omits the important elements Na, K, and Fe, it is a system for which a considerable body of thermodynamic data exists. By combining melt-absent phase diagrams calculated from available thermodynamic data bases with the experiments, we have constructed a model that can easily be extended to natural basaltic and intermediate rock compositions.

The upper pressure subsolidus stability limit of aluminous amphibole (Amp) + quartz (Qtz) in CMASH near 25 kb is delineated by an H_2O-conserving reaction generating Tal + Kya + Zoi + Cpx and also by dehydration reactions. When H_2O is part of the low-temperature high-pressure assemblages, this indicates both backbending (where $\Delta V = 0$) and downbending (where $\Delta S = 0$) of dehydration reactions that have positive dP/dT at lower pressure.

Talc + zoisite (Zoi) + quartz (Qtz) is stable only in the vicinity of the H_2O-saturated solidus for a small range near 20 to 25 kb. Epidote amphibolites (Amp + Zoi + Qtz + (plagioclase) Plg are stable from about 8 to 20 to 25 kb and undergo dehydration-melting in thickened continental crust and in subducted oceanic lithosphere. This occurs at temperatures below 800°C—much lower temperatures than the fluid-absent melting of amphibolite (Amp + Plg/(garnet) Gar + Qtz). The assemblage Tal + Amp + Plg + Qtz only undergoes dehydration-melting at low pressures (near 6 kb) at about 750° to 800°C. Although the amount of melt produced by dehydration-melting of epidote + amphibole (Zoi + Amp + Qtz + Plg/Gar) is small compared to that produced by dehydration-melting of amphibolite (Amp + Qtz + Plg/Gar), these relatively low temperature melts could be important both in

* Department für Erdwissenschaften, E.T.H. Zürich, Switzerland CH-8092.
** Department of Geology, The Australian National University, GPO Box 4, Canberra City, ACT 2601, Australia.

collision belts and in subducted oceanic crust. Magmatic epidote has been reported from granitic rocks formed in rapidly exhumed thickened crust.

Melt production by dehydration-melting of Amp ± Zoi will be minimal close to the intersections of the appropriate reactions near 25 kb, 800°C close to the H_2O-saturated solidus. Melt amount increases continually down the high-pressure dehydration-melting curve of aluminous-Amp (to garnet + clino- + ortho-pyroxene + quartz + melt) which has a negative dP/dT. Melt production is maximum close to 900°C between about 5 to 15 kb, when anorthite replaces garnet in the above assemblage. These latter "lower-pressure" melts could be erupted. The former "higher pressure" melts (15-20 kb) would tend to precipitate amphibole which may impede their ascent. At pressures higher than the stability of plagioclase (± quartz) all initial melts (whether H_2O-saturated or -undersaturated) are peraluminous and very siliceous. This contrasts to lower pressure melting where H_2O-saturated melts are peraluminous and where H_2O-undersaturated melts are meta- to sub-aluminous.

The simultaneous dehydration-melting of zoisite and amphibole will induce melting close to their intersection with the H_2O-saturated CMASH "basaltic" solidus near 25 kb, 800°C. This region in CMASH coincides with the dehydration of talc. In ultramafic systems a similar region overlaps the dehydration of serpentine near 25 kb, 700°C. Thus subduction zone PT-paths passing through this region will encounter dehydration of both hydrated mantle and oceanic crust at about the same time, considerably enhancing melt production.

INTRODUCTION

The development of oceanic and continental crust is directly related to melting of ultramafic mantle or remelting of derived basalt (hydrated to amphibolite, presumably at mid-ocean ridges), respectively.

Despite reconnaissance experiments on natural compositions, the systematics of dehydration and hydrous melting (including dehydration-melting) of mafic and ultramafic rocks is poorly understood. The system CaO + MgO + Al_2O_3 + SiO_2 (CMAS) has long been used by petrologists as a suitable simplified system for investigating melting and crystallization of peridotitic mantle and of basaltic liquids (Chinnner and Schairer, 1962; O'Hara, 1965, 1968; Humphries, Biggar, and O'Hara, 1972). Although it could be argued that the study of simple systems has limited direct applications to specific natural rock compositions, it is still extremely useful and necessary to understand properly these systems. More comprehensive petrogenetic grids for mafic-intermediate composition source rocks require thermodynamic quantification of extremely complex crystalline solutions and partial melts. Thus it has been demonstrated that the production of corundum-normative silicic melts from a diopside-normative source rock is possible in the presence of excess water within the plagioclase stability field (see Ellis and Thompson, 1986; Conrad, Nicholls, and Wall, 1988, for review). The demonstration of this feature in such a simple system as CMASH therefore provides a means of

explanation for this phenomenon in natural rocks without immediate recourse to the effects of the more complex and additional components.

In this paper we present the results of subsolidus, water excess melting, and dehydration-melting experiments for the silica-excess $CaO + MgO + Al_2O_3 + SiO_2 + H_2O$ (CMASH) system beyond the stability of anorthite ($\sim$ 15 kb) up to 35 kb pressure. This chemical system serves as a simplified background against which we can advance to more complex compositions to systematize the high-grade metamorphism and melting of mafic and ultramafic rocks. The silica-excess region is relevant to the melting of many amphibolites. Because of the low silica content of many amphiboles even olivine normative basalt, when converted to amphibolite (Thompson, Laird, and Thompson, 1982) or eclogite (D. H. Green and Ringwood, 1967b), contains quartz.

Calculations of the P-T locations of melt-free equilibria (with the program VERTEX, Connolly, 1990, using two recent thermodynamic data bases [Berman, 1988; Holland and Powell, 1990]) have been compared with the experimental results. Despite adolescent discrepancies, the results of the calculations encourage us to extend such work toward the relevant natural compositions.

CMASH AS A MODEL SYSTEM FOR METAMORPHISM AND MELTING OF MAFIC ROCKS

CMASH has proved a useful system to model the metamorphism of ultramafic rocks (Jenkins, 1981, 1983; Obata and Thompson, 1981). Because mafic magmas fractionate toward Na and Fe richer compositions, a large spectrum of differentiates can be related to a more primitive magma composition. The metamorphism of such rocks can be adequately represented by CMASH either if they are early differentiates (that is low in Na, Fe) or the assemblage contains plagioclase and magnetite, to buffer the additional components.

The quartz-bearing region of CMASH has proved useful as a model system for metamorphism (Jenkins, 1981, 1983; Obata and Thompson, 1981) and for melting of mafic compositions (amphibolites and eclogites) to produce intermediate and felsic magmatic rocks (Ellis and Thompson, 1986). The CMASH system contains important endmembers for most of the common rock forming minerals in metamorphosed mafic (basaltic) compositions (table 1).

The near solidus and melting relations in CMASH to 15 kb, for a wide range of $aSiO_2$ (from quartz to forsterite saturation), have been examined by Ellis and Thompson (1986) for anorthite-bearing mineral assemblages. We found that the "norite" thermal divide (Anr + Opx $\pm$ Qtz) separating diopside-normative from corundum-normative eutectic melts at low pressure was broken at successively lower temperatures with increasing P_{H_2O} and a_{H_2O}. This permitted subaluminous clinopyroxene or amphibole to coexist with corundum-normative melts. At higher pressures beyond the stability of plagioclase the melting reactions must, of course, be of a completely different nature as, by definition, the norite

TABLE 1

List of abbreviations for CMASH phases

Amp	amphibole	
Anr	anorthite	$CaAl_2Si_2O_8$
Cos	coesite	SiO_2
Cor	corundum	Al_2O_3
Cats	Ca-Tschermaks molecule	$CaAl_2SiO_6$
Chl	chlorite	
Cl	chlinochlore	$(Mg_5Al)(Si_3Al)O_{10}(OH)_8$
Cp	corundophyllite	$(Mg_4Al_2)(Si_2Al_2)O_{10}(OH)_8$
Cpx	clinopyroxene	
Crd	cordierite	$Mg_2Al_3(Si_5Al)O_{18}$
Dio	diopside	$CaMgSi_2O_6$
Ens	enstatite	$MgSiO_3$
For	forsterite	Mg_2SiO_4
Gar	garnet	
Gro	grossular-rich garnet	$Ca_3Al_2Si_3O_{12}$
Ca_2Mg-Gar		$Ca_2MgAl_2Si_3O_{12}$
$CaMg_2$-Gar		$CaMg_2Al_2Si_3O_{12}$
H-Crd	hydrous cordierite	
Kya	kyanite	Al_2SiO_5
L	liquid	
Opx	orthopyroxene	
Py	pyrope	$Mg_3Al_2Si_3O_{12}$
Pyp	pyrope-rich garnet	
Qtz	quartz	SiO_2
Sap	sapphirine	$Mg_2Al_4SiO_{10}$
Sil	sillimanite	Al_2SiO_5
Spn	spinel	$MgAl_2O_4$
Tal	talc	$Mg_3Si_4O_{10}(OH)_2$
Tr	tremolite	$Ca_2Mg_5Si_8O_{22}(OH)_2$
Tt		$Ca_2(Mg_4Al)(Si_7Al)O_{22}(OH)_2$
Ts	tschermakite	$Ca_2(Mg_3Al_2)(Si_6Al_2)O_{22}(OH)_2$
Trd	tridymite	SiO_2
V	vapor	(close to H_2O)
Wol	wollastonite	$CaSiO_3$
Zoi	zoisite	$Ca_2Al_3Si_3O_{12}(OH)$

divide cannot exist. Of particular interest is whether the derivation of corundum-normative melts from diopside-normative sources at high P_{H_2O}, which we observed in the presence of plagioclase, would also occur at higher pressures in the absence of feldspar.

The relationship of H_2O-saturated experiments to melting of mafic assemblages needs special consideration at higher pressures (15-35 kb) where reactions involving talc and zoisite, in addition to amphiboles, in CMASH will generate new dehydration-melting reactions which define

the evolution of H_2O-undersaturated melts. The study provides in addition much information on the stability limit for fluid-absent (dehydration-melting) of Ca-amphibole in mafic compositions in the specific tectonic environments of continental collision and subduction zones. It also focusses attention on the transport of H_2O in subduction zones deeper than the stability of amphibole.

Our experimental results in CMASH are grouped into specific P-T regions:

1. at pressures from 2 to about 10 kb and temperatures from the H_2O-saturated solidus to amphibolite dehydration melting, to examine the crystallization of hydrous mafic and derivative magmas within continental crust of normal thickness (continuing the discussions from Ellis and Thompson, 1986);
2. at pressures from about 10 to 25 kb to examine the role of amphibolite melting in thickened lower crust and subducted oceanic crust;
3. phase relations close to the H_2O-saturated solidus from 5 to 30 kb to understand the role of other common hydrous minerals (here zoisite and talc);
4. solidus reactions in coesite eclogites including the disappearance of amphibole.

PHASE RELATIONS IN RELATED SYSTEMS

Previous experimental work in subsystems of CMASH provide important background information for the present study.

$CaO + MgO + Al_2O_3 + SiO_2$ (CMAS)

The $CaO + MgO + Al_2O_3 + SiO_2$ (CMAS) system (anhydrous) has been extensively studied as a model for the gabbro–garnet granulite–eclogite transitions in quartz-excess rocks (Hensen, 1976; Hansen, 1981; Perkins, 1983), the plagioclase–spinel–garnet transitions in ultramafic rocks (Kushiro and Yoder, 1966) and its liquidus phase relations (Liu and Presnall, 1990).

The results in CMAS have been well summarized by Irvine and Sharpe (1982) and by Harley and Carswell (1990). The two anhydrous reactions (mineral abbreviations are given in table 1, reactions discussed are listed in table 2):

$$\text{Anr} + \text{Opx} = \text{Pyp} + \text{Cpx} + \text{Qtz} \quad (1)$$

and

$$\text{Pyp} + \text{Anr} + \text{Qtz} = \text{Cpx} + \text{Kya} \quad (2)$$

subdivide quartz-excess mafic rocks in CMAS into three fields—the two pyroxene granulite, the garnet granulite, and the eclogite facies (fig. 1A). These experimental studies have outlined the various subsolidus reac-

tions involving orthopyroxene (Opx), clinopyroxene (Cpx), pyrope-rich garnet (Pyp), kyanite (Kya), anorthite (Anr), and quartz (Qtz). Because of the sluggish nature of reactions in laboratory experiments on dry systems, most of these studies have been restricted to high temperatures. The location of such equilibria at lower temperatures, applicable to crustal conditions, has necessitated extrapolation (the linear extrapolated eclogite stability field of D. H. Green and Ringwood, 1967b) to low pressures and the more recent curved extrapolations by several workers (Wood, 1987; Harley and Carswell, 1990, p. 54). These limit eclogite formation to the base of the crust thickened to more than 35 km and to mafic compositions in the mantle.

The presence of water in the CMAS system has the effect of stabilizing hydrous minerals and of lowering the solidus temperature with increasing pressure while anorthite is stable. This occurs because OH- destabilizes Si–O bonds in tectosilicates and derived melts. In addition with water, faster reaction rates permit experiments to be undertaken at considerably lower temperatures than in the dry system. Although reactions (1) and (2) are univariant reactions in the CMAS system, petrologic and geophysical implications of these P-T boundaries (Kushiro and Yoder, 1966) have been questioned by several workers (for example, Ringwood and D. H. Green, 1966) because of the considerable effects of other components (Na_2O, FeO) on displacing these reactions from a unique P-T line to a broad reaction interval at crustal pressures.

The presence of water has an effect on the compatibilities of these reactions and assemblages especially in Fe- and alkali-bearing systems because of the stability of chemically complex hydrous minerals (for example, amphibole, talc, and zoisite). These additional phases have the effect of eliminating many of the proposed anhydrous reactions over crust and upper mantle P-T conditions. Hydrous minerals will modify the mineralogical nature and pressure-temperature conditions of the gabbro–garnet granulite–eclogite transitions in the greenschist, amphibolite, and blueschist facies. For example, the reaction (1) of anorthite and orthopyroxene to garnet and clinopyroxene is restricted to temperatures higher than 925°C in the hydrous (CMASH) system (see Ellis and Thompson, 1986) because of the appearance of amphibole.

$CaO + Al_2O_3 + SiO_2 + H_2O$ (CASH)

Some of the phase relations in CASH determined by Boettcher (1970) are also included in figure 1, A and B. They provide limits in the MgO-free system to water-saturated melting at various pressures, particularly regarding the stability limits of anorthite with water and of zoisite (with or without quartz). It can be anticipated from the superimposed curves in figure 1 that the reactions producing pyrope-rich garnet from anorthite-bearing assemblages will be replaced at higher pressures by zoisite reactions in the CMASH system.

TABLE 2

The reactions discussed in this paper

Anr + Opx = Pyp + Cpx + Qtz	(1)
Pyp + Anr + Qtz = Cpx + Kya	(2)
Tre = Di + Ens + Qtz + V	(3)
Tal = Ens + Qtz + V	(4)
Tre = 2Dio + Tal	(5)
Zoi + Amp + Kya + Qtz + V = L	(6)
Zoi + Pyp +Kya + Qtz + V = L	(7)
Zoi + Cpx +Kya + Qtz + V = L	(8)
Amp + Qtz + V = Cpx + Opx + L	(9)
Amp + V = Pyp + Cpx + Opx + L	(10)
Amp + Zoi + V = Pyp + Cpx + L	(11)
Zoi + Tal + Pyp + Cpx = Amp + Qtz	(12)
Zoi + Tal + Kya + Cpx = Amp + Qtz	(13)
Cpx + Tal + Kya = Amp + Qtz + Pyp	(14)
Amp = Pyp +Tal +Cpx + Qtz +V	(15)
Amp + Qtz = Tal + Kya + Cpx + V	(16)
Tal + Cpx + Zoi = Amp + Qtz +V	(17)
Cpx + Pyp + Cos + Zoi + V = L	(18)
Zoi + Pyp + Cos + V = Cpx + L	(19)
Zoi + Amp + Cos = Cpx + Kya + V	(20)
Zoi + Pyp + Cos = Cpx + Kya + V	(21)
Cpx + Kya + Qtz + V = Opx + L	(22)
Cpx + Opx + Kya + V = Pyp + L	(23)
Gro + Cpx + Anr + Qtz + V = L	(24)
Gro + Cpx + Zoi + Qtz + V = L	(25)
Amp = Anr + Opx + Cpx + Qtz + L	(26)
Amp = Pyp + Cpx + Opx + Qtz + L	(27)
Amp = Pyp + Cpx + Opx + Qtz + V	(28)
Amp + V = Anr + Cpx + Opx + L	(29)
Zoi + Amp + Qtz = Anr + Cpx + L	(30)
Zoi + Amp + Qtz = Cpx + Pyp + L	(31)
Zoi + Amp + Qtz = Cpx + Kya + L	(32)
Anr + Amp + Qtz = Pyp+ Cpx + L	(33)

$CaO + MgO + SiO_2 + H_2O$ (CMSH)

Both tremolite and talc are represented in the simple system CMSH (fig. 1B). Experimental work and calculation of the dehydration reactions of talc and tremolite to high pressures and temperatures have been

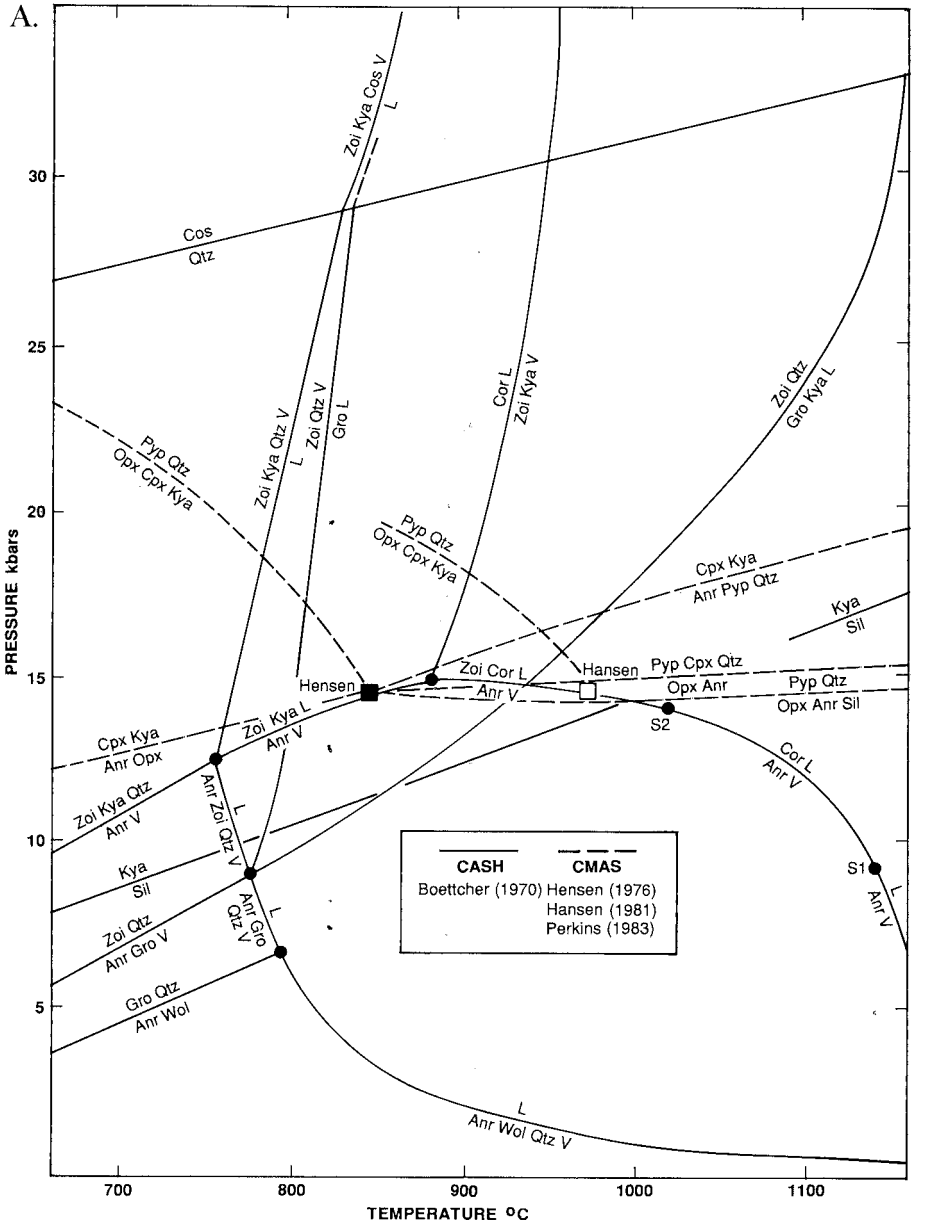

Fig. 1. Pressure-temperature diagrams showing the H_2O-saturated solidii and some sub-solidus reactions in the limiting systems MSH, CASH, CMSH. Also plotted in (A) are the reactions in CMAS among Pyr, Qtz, Anr, Opx, and Al_2SiO_5 from Hensen (1976), Hansen (1981), and Perkins (1983) and reactions involving zoisite and anorthite + H_2O in CASH from Boettcher (1970). In (B) the calculated dehydrations of talc and tremolite are shown extrapolated from low pressure brackets by Essene, Wall, and Shettel (E, W, S; 1974, see Vernon, 1976), by Delaney and Helgeson (D, H; 1978) and by Jenkins, Holland, and Clare (J; 1991); the water-conserving reaction Tre = Dio + Tal from Essene, Wall, and Shettel

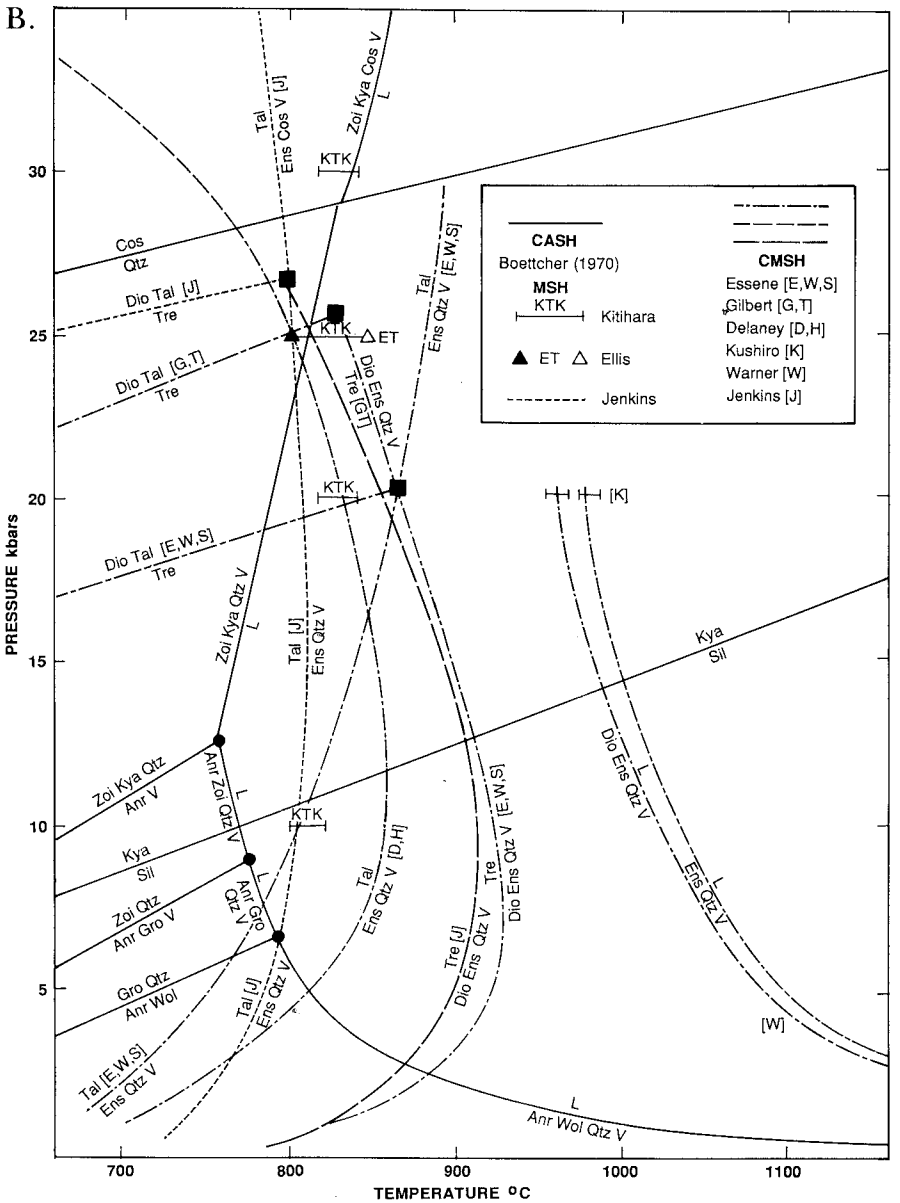

Fig. 1(continued) (E, W, S; 1973), Gilbert and Troll (G, T; 1982) and Jenkins, Holland, and Clare (J; 1991); the eutectic melting reactions Dio + Ens + Qtz + V = L and Ens + Qtz + V = L at 20 kb from Kushiro (K; 1969) and at low pressures from Warner (W; 1975). The quartz (Qtz) – coesite (Cos) transition is from Boettcher and Wyllie (1968) and the kyanite (Kya)-sillimanite (Sil) boundary from Richardson, Gilbert, and Bell (1969) are also shown. Experimental data obtained here on the upper temperature stability limit of talc (filled triangle) relative to enstatite + quartz + H_2O (open triangle) at 25 kb are also shown (are consistent with the results of Kitahara, Takenouchi, and Kennedy (1966), solid bars at 10, 20, and 30 kb, labelled KTK).

recently summarized by Jenkins, Holland, and Clare (1991). The upper temperature limit of tremolite is defined in CMSH by the dehydration reaction

$$\text{Tre} = \text{Di} + \text{Ens} + \text{Qtz} + (H_2O)V \quad (3)$$

The calculated location of this reaction by Essene, Wall, and Shettel (1973) and by Jenkins, Holland, and Clare (1991) agree with the experimental results of Gilbert and Troll (1974, as summarized by Jenkins, Holland, and Clare, 1991, p. 459, Gilbert and others, 1982, p. 254, 268).

Calculations and experiments relevant to the upper thermal stability limit of talc defined by the reaction

$$\text{Tal} = \text{Ens} + \text{Qtz} + (H_2O)V \quad (4)$$

are shown in figure 1B. This curve, as calculated by Essene, Wall, and Shettel (1973), extrapolates close to 900°C at high pressure (25 kb) with a positive dP/dT slope. The calculated location by Delaney and Helgeson (1978) has a strong back-bending limiting its stability to 800°C at 25 kb, with maximum thermal stability around 10 kb. The pressure of backbending of such reactions probably reflects as much the values chosen for compressibility of the hydrous minerals rather than the differences in the equation of state for water used (T. J. B. Holland, personal communication, May 1992; see also app. 2, fig. A1, A and B). The thermodynamic data base of Holland and Powell (1990) gives a maximum talc stability (reaction 4) at about 810°C at 20 kb, intermediate between the above two estimates (see Jenkins, Holland, and Clare, 1991, p. 459). Our new experimental data on talc stability (table 3, runs Z-18, Z-27, T-1394) bracket the upper stability limit of talc to between 800° and 850°C at 25 kb agreeing with the results of Kitahara, Takenouchi, and Kennedy (1966) and more recent studies as summarized by Jenkins, Holland, and Clare (1991, p. 459).

Previous calculations by Essene, Wall, and Shettel (1973; reported by Vernon, 1976, p. 117) indicated that the dehydration reactions (3 and 4) intersect at the H_2O-conserving reaction among tremolite-diopside-talc in the vicinity of 20 kb at 860°C to 27 kb at 790°C in figure 1B

$$\text{Tre} = 2\text{Dio} + \text{Tal} \quad (5)$$

The eutectic melting reaction (fig. 1B) among diopside + enstatite + quartz + H_2O occurs near 960°C at 20 kb (Kushiro, 1964, fig. 7) and near 1090°C at 5 kb (Warner, 1975). Thus it would not be expected that tremolite or talc dehydration curves would intersect the appropriate water-saturated eutectic melting curves in CMSH. However, because the addition of aluminium to CMSH permits the appearance of anorthite below about 12 kb, the quartz and H_2O-saturated solidus in CMASH (Ellis and Thompson, 1986) will lie at temperatures just below that in CASH (the eutectic melting reaction Anr + Qtz + V = L, Stewart, 1967) (fig. 1).

PHASE COMPOSITIONS AND REACTIONS IN CMASH EXPERIMENTS AT QUARTZ AND WATER EXCESS CONDITIONS FROM 15 TO 35 KB

Our experiments were conducted for several compositions in CMASH from 15 to 35 kb and from 700° to 1000°C to examine the dehydration and melting behavior of model amphibolite and hydrous eclogite in thickened crust and in subduction zones. Details of the experimental methodology and starting mix compositions are presented in app. 1, and the results of the experiments are presented in table 3.

The compositions of ideal endmember phases and crystalline solutions, together with analysed synthetic phases and starting-mix compositions (app. 1, table A-1), are shown in two projections in figure 2. The ACM diagram (Al_2O_3 + CaO + MgO) projected from SiO_2 and H_2O in figure 2A is applicable to the subsolidus region and that immediately above the quartz- and water-saturated solidus. The $CaAl_2SiO_6$ + Mg_2SiO_4 + SiO_2 diagram projected from $CaMgSi_2O_6$ and H_2O (the basal plane of the basalt tetrahedron in CMASH, fig. 2B) is also very useful to understand some of the deduced reactions, especially because the formation of siliceous liquids (due to melting at high H_2O-contents) commonly removes quartz from the assemblages.

Of the phases considered, amphiboles and melt show the greatest compositional variation in the P-T range studied (fig. 2 and table 4). The amphiboles show some [$CaMg_{-1}$] variation as do Gar (Pyr and Gro), Cpx, and Opx. Amp also shows much larger variation in [$Al_2Mg_{-1}Si_{-1}$] than Cpx or Opx (fig. 2). Buffering assemblages for [$Al_2Mg_{-1}Si_{-1}$] such as Anr + Cpx + Qtz; Zoi + Kya + Cpx + Qtz + H_2O (see below) were not present over a large enough range of P-T space to permit useful calibration of variation in $Al_2Mg_{-1}Si_{-1}$ [Amp] in these assemblages. Likewise Amp was rarely found with Gar + Cpx (or Opx) or with Gar + Kya + Qtz at higher pressures for the compositions and the P-T range studied. Some of the amphiboles exhibit apparent cation deficiency (see app. 1). This was earlier attributed by Oba (1978, p. 343) to the substitution $2Al^{VI} = 3$ Mg in tschermakitic amphiboles synthesized by him at 15 and 20 kb at 850°C (see also Cho and Ernst, 1991). However, unlike the analyses reported by Oba (1978), none of the amphiboles synthesized here in quartz-rich compositions was more aluminous than (tt) $Ca_2(Mg_4Al)(Si_7Al)(Si_7Al)O_{22}(OH)_2$. The best analyses here were selected on the basis of stoichiometry (see app. 1). Without using this criteria for "good" data, it is almost impossible to tell if it is a "real" amphibole analysis or else contamination from another phase or melt.

We have attempted to work out the complete stable reaction grid for CMASH to 35 kb from 700° to 1000°C by comparing our experimental results with calculations of melt-absent reactions obtained with recent thermodynamic data bases (These calculations are presented in app. 2 as they are independent of the present experimental results). As discussed below, the present comparison leaves much room for improvement. Rather than discuss each reaction in turn, we find it most useful to focus on specific P-T regions (figs. 3 and 4) and families of reactions (table 2),

TABLE 3

Experimental run conditions and run products

RUN	P (Kb)	T (°C)	TIME (hours)	STARTING COMPOSITION	RUN PRODUCT
Z-2	20	900	17	CASH oxides+15%H_2O	Zoisite
Z-4	30	1000	101	Al	Cpx Gar Zoi (Qtz)
Z-4	30	1000	101	B1	Cpx Gar Zoi Qtz Liq
Z-10	30	1100	1.3	CMS oxide mix	Diopside
Z-11	20	700	262	A2+4%H_2O	Cpx Zoi Qtz V (Tr?)
				B2+4%H_2O	Cpx Gar Zoi Qtz V
Z-13	20	800	146	E2+19%H_2O	Cpx (trace) Zoi St (Liq?)
Z-14	30	700	121	A2+18%H_2O	Cpx Gar Zoi Qtz V
				B2+19%H_2O	Cpx Gar Zoi Qtz V
				E2+17%H_2O	Cpx Zoi Tc Qtz V
Z-15	30	800	168	A2+22%H_2O	Cpx Zoi Ky Qtz V
				B2+19%H_2O	Cpx Gar Zoi Qtz V
				E2+16%H_2O	Cpx Gar Ky Qtz V
Z-16	35	800	126	A2+18%H_2O	Cpx Zoi Ky (Qtz?) V
				B2+18%H_2O	Cpx Gar Zoi Qtz Liq (v)
				E2+20%H_2O	Cpx Gar Ky Zoi (Qtz) V
Z-17	15	800	124	A2+24%H_2O	Cpx Zoi Qtz V
				B2+19%H_2O	Cpx Gar Zoi Qtz Liq
				E2+19%H_2O	Gar Tr Zoi Qtz
Z-18	25	800	99	A2+23%H_2O	Cpx Zoi Tc (Qtz?) V
				B2+23%H_2O	Cpx Gar Zoi Qtz Liq
				E2+23%H_2O	Zoi Tc
Z-19	25	900	64	A2+17%H_2O	Cpx Gar Zoi V
				B2+18%H_2O	Cpx Gar Zoi Liq V
				E2+17%H_2O	Cpx Gar Zoi V
Z-21	25	700	497	A2+23%H_2O	Cpx Zoi Tc Qtz V
				B2+23%H_2O	Cpx Gar Zoi Qtz V
				E2+25%H_2O	Cpx Zoi Tc Qtz V
Z-22	30	900	47	A3+20%H_2O	Cpx Gar Zoi Liq V
				B3+23%H_2O	Cpx Gar Zoi Liq V
				E3+22%H_2O	Cpx Gar (Qtz) Liq V
Z-23	20	900	96	A3+21%H_2O	Cpx Zoi Liq V
				B3+24%H_2O	Cpx Gar Zoi Liq V
				E3+23%H_2O	Cpx Gar Zoi Liq

TABLE 3
(continued)

RUN	P (Kb)	T (°C)	TIME (hours)	STARTING COMPOSITION	RUN PRODUCT
Z-24	15	900	47	A3+24%H_2O	Cpx Qtz Liq
				B3+23%H_2O	Cpx Zoi Liq V
				E3+23%H_2O	Cpx Tr Liq V
Z-26	20	1000	19	$MgSiO_3$ oxide	Enstatite
Z-27	25	800		B3+23%H_2O	Cpx Gar Zoi Qtz V
				E4+22%H_2O	Tr Zoi Tc (Qtz) V
Z-28	20	800	144	E4+25%H_2O	Tr Zoi Cpx Qtz V
				B3+22%H_2O	Cpx Gar Zoi Qtz V
Z-29	20	850	81	A3+24%H_2O	Cpx Tr Qtz Liq V
				B3+23%H_2O	Cpx Gar Zoi Liq V
Z-30	25	850	75	B3+23%H_2O	Cpx Gar Zoi Qtz
				E3+25%H_2O	Cpx Tr Ky Qtz V
Z-31	28	800	116	A4+24%H_2O	Cpx Ky (Tc) Qtz V
				E3+24%H_2O	Cpx Ky Tc Qtz V
Z-32	28	850	66	B3+22%H_2O	Cpx Zoi Qtz Liq V
Z-33	28	850	72	A4+26%H_2O	Cpx Ky Liq V
				E3+30%H_2O	Cpx Ky Qtz V
Z-34	15	850	71	E3+23%H_2O	Zoi Tr Liq V
Z-35	27	850	72	A4+21%H_2O	Cpx Opx Ky Qtz V
Z-36	25	875	43	A4+23%H_2O	Cpx Gar Opx Qtz Liq V
				E3+23%H_2O	Cpx Ky Qtz Liq (V)
Z-38	20	875	67	A4+25%H_2O	Cpx Gar Tr (Liq) V
				E3+21%H_2O	Gar Tr Liq V
Z-39	15	925	25	A4+27%H_2O	Cpx Opx Qtz Liq V
				E3+25%H_2O	Tr Cpx (Opx) Liq V
Z-44	35	850		A4+30%H_2O	Gar Opx (Cpx) V
				B3+24%H_2O	Cpx Gar Zoi Liq V
				E3+29%H_2O	Cpx Ky V
Z-45	28	825	121	A4+31%H_2O	Cpx Opx Qtz V
				E3+37%H_2O	Cpx Ky Qtz V

TABLE 3
(continued)

RUN	P (Kb)	T(°C)	TIME	STARTING COMPOSITION	RUN PRODUCT
T-980	30	1000	146	$Py_{70}Gr_{30}$-Zoi-Qtz	Gar Cpx Ky Qtz V
T-981	25	850	143	" + 20%H_2O	Gar Kya Liq V
T-1023	35	900	42	" + 15%H_2O	Gar Cpx Liq V
T-1055	35	900	121	" + 15%H_2O	Gar Cpx Liq V
T-1201	15	950	27	E + Qtz + 25%H_2O	Cpx Opx Liq V
T-1203	25	850	90	Amp+Qtz oxides+23%H_2O	Gar Cpx Opx Liq V
T-1204	27	850	90	Amp+Qtz oxides+21%H_2O	Gar Cpx Opx Liq V
T-1231	20	900	67	Amp+Qtz oxides+20%H_2O	Gar Cpx Opx Liq V
T-1235	23	850	68	Amp+Qtz oxides+20%H_2O	Gar Cpx Opx Liq V
T-1244	17	850	93	Amp+Qtz oxides+19%H_2O	Amp Qtz V
T-1392	10	750	18	Talc oxides+15%H_2O	Talc V
T-1394	25	850	18	Talc (T-1392)	Ens Qtz V
T-1396	17	850	125	Amp+Qtz oxides+19%H_2O	Amp Qtz
T-1402	23	950	169	Amp Qtz (T-1396)	Gar Cpx Opx Liq
T-1405	23	925	245	Amp Qtz (T-1396)	Gar Cpx Opx Liq (Kya)
T-1416	23	900	569	Amp Qtz (T-1396)	Gar Cpx Opx L
T-1439	17	850	73	Amp + Qtz oxides+15%H_2O	Amp Qtz V
T-1445	23	875	216	Amp Qtz (T-1439)	Gar Cpx Opx L

which illustrate best the metamorphism and melting of mafic rocks in specific tectonic environments. The areas to be discussed in detail are indicated by the boxed regions in figure 4. The most significant parts of the CMASH phase diagram are those defined by the occurrence of one or more of the hydrous minerals (Amp, Zoi, Tal) relative to melting reactions (either H_2O-saturated or fluid-absent).

H_2O-saturated solidus phase relations from 15 to 25 kb (a model for amphibolite melting under H_2O-excess conditions.—Phase relations in CMASH to 10 kb have been discussed by Ellis and Thompson (1986)—region (1) in figure 4. Although the overall interpretation of experiments in this paper also uses data from that work, only the results from 15 to 35 kb are presented in detail here. Table 3 and figure 2A,B show the compositions of coexisting phases obtained in the higher pressure experiments.

The major difference from the lower pressure experiments of Ellis and Thompson (1986) is that for rocks of basaltic compositions in CMASH, with excess quartz and H_2O, above about 12 kb anorthite is no longer stable (figs. 1A, 3, and 4), being replaced by zoisite assemblages. Another difference concerns the stability of the assemblage Tal + Zoi + Qtz. According to the results of calculation of subsolidus equilibria with

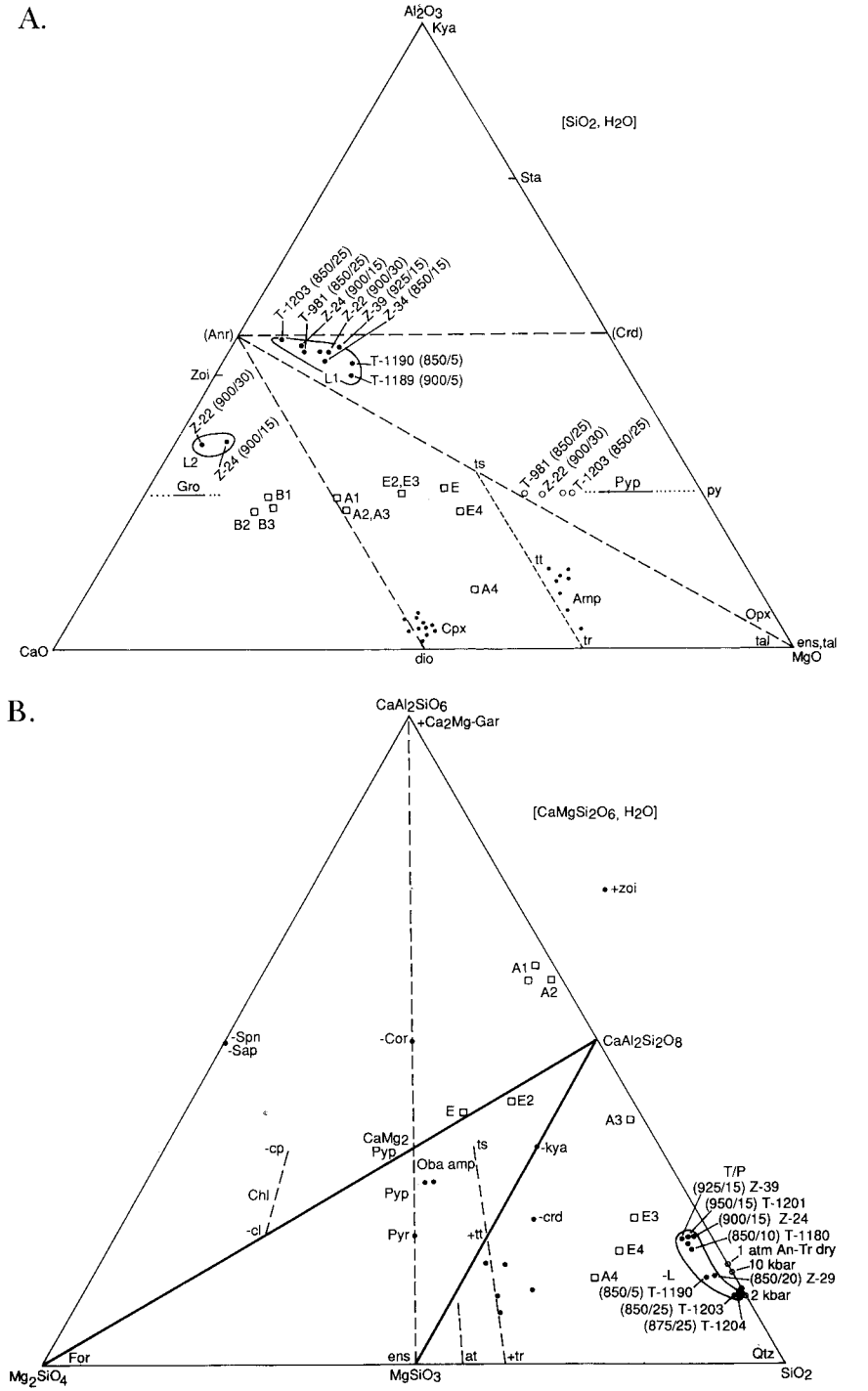

Fig. 2. The compositions of phases in CMASH and the compositions of minerals and glasses synthesized in the experiments (tables 3 and 4, identified by run number and T°C/Pkb). (A) These are shown in a molar projection from SiO_2 and H_2O onto the ACM plane (Al_2O_3 + CaO + MgO) and (B) a molar projection from $CaMgSi_2O_6$ and H_2O onto Mg_2SiO_4 + SiO_2 + $CaAl_2SiO_6$. The open squares denote starting mix compositions (see table A1). The enclosed points labelled L1, L2 represent analysed glasses, and Cpx, Amp, Oba, Amp and Gar are mineral analyses. The compositions of the anorthite + quartz + H_2O eutectic liquids to 10 kb (Stewart, 1967) are shown in B. In (B) the negative prefix indicates compositions lying below the plane of projection.

TABLE 4

Compositions of minerals and melts from selected experiments

Phase	Gar	Cpx	Tr	Tr	Cpx	Cpx	Cpx	Cpx	Cpx	Gar	Cpx	Cpx
Run No	Z-4A	Z-4A	Z-13E	Z-13E	Z-13E	Z-15A	Z-15A	Z-15A	Z-15B	Z-15B	Z-15E	Z-16B
P Kbar/T°C	30/1000	30/1000	20/800	20/800	20/800	30/800	30/800	30/800	30/800	30/800	30/800	35/800
SiO_2	43.93	50.05	52.31	51.48	54.94	53.48	54.44	54.48	53.82	40.59	54.52	54.17
Al_2O_3	24.00	11.63	10.19	10.23	1.38	5.21	3.57	1.59	2.75	22.80	1.92	2.91
MgO	18.89	14.32	20.97	20.11	18.99	16.36	17.32	18.18	17.26	0.61	18.41	17.17
CaO	13.18	24.64	12.55	13.76	24.75	24.95	24.67	25.52	25.93	35.73	25.14	25.43
Total	100.00	100.64	96.02	95.58	100.06	100.00	100.00	99.77	99.76	99.73	99.99	99.68
Si	3.055	1.783	7.190	7.143	1.972	1.918	1.951	1.963	1.942	3.025	1.961	1.950
Al	1.967	0.488	1.651	1.673	0.058	0.220	0.151	0.063	0.117	2.003	0.082	0.124
Mg	1.958	0.760	4.295	4.158	1.016	0.875	0.925	0.976	0.928	0.068	0.987	0.921
Ca	0.982	0.941	1.848	2.046	0.952	0.959	0.947	0.986	1.002	2.854	0.969	0.981
Cation total	7.962	3.973	14.985	15.020	3.999	3.972	3.974	3.998	3.989	7.950	3.999	3.976
No. of oxygens	12	6	23	23	6	6	6	6	6	12	6	6
A	25.08	12.55	11.8	11.9	1.5	5.7	3.9	1.7	2.9	25.5	2.1	3.2
C	25.03	48.35	26.5	29.1	47.7	49.3	48.6	49.4	50.4	72.7	48.5	49.9
M	49.89	39.09	61.7	59.1	50.9	45.0	47.5	48.9	46.7	1.7	49.4	46.9
X_{Ca}^{Gar}	0.33									0.97		

Phase	Gar	Cpx	Gar	Gar	Cpx	Cpx	Tr	Tr	Cpx	Cpx	Cpx	Gar
Run No	Z-16B	Z-16E	Z-16E	Z17-B	Z-17B	Z-17B	Z-17E	Z-17E	Z-19A	Z-19A	Z-19A	Z-19A
P Kbar/T°C	35/800	35/800	35/800	15/800	15/800	15/800	15/800	15/800	25/900	25/900	25/900	25/900
SiO_2	41.13	54.12	43.00	42.58	55.41	55.15	51.57	52.87	53.24	54.20	53.82	43.27
Al_2O_3	21.59	3.64	24.83	20.33	1.41	5.13	12.22	11.82	4.92	3.55	5.33	24.88
MgO	1.35	17.90	21.23	3.08	18.85	16.30	20.02	21.40	17.19	17.74	16.83	22.81
CaO	35.95	24.34	10.95	32.97	26.55	25.99	13.18	13.27	24.64	24.50	24.21	10.35
Total	100.02	100.00	100.01	98.96	102.22	102.57	96.99	99.36	99.99	99.99	100.19	101.31
Si	3.066	1.939	2.978	3.173	1.957	1.929	7.031	7.039	1.911	1.943	1.921	2.957
Al	1.898	0.154	2.027	1.786	0.059	0.212	1.964	1.855	0.208	0.150	0.224	2.004
Mg	0.150	0.956	2.192	0.342	0.992	0.850	4.068	4.246	0.919	0.948	0.895	2.323
Ca	2.871	0.934	0.813	2.633	1.005	0.974	1.925	1.893	0.947	0.941	0.926	0.758
Cation total	7.985	3.983	8.010	7.934	4.013	3.965	14.987	15.033	3.985	3.982	3.967	8.041
No. of oxygens	12	6	12	12	6	6	23	23	6	6	6	12
A	23.9	3.9	25.2	23.1	1.4	5.5	14.1	13.1	5.3	3.8	5.8	24.5
C	72.3	47.5	20.2	68.1	49.6	50.5	27.6	26.8	48.1	47.9	47.9	18.5
M	3.8	48.6	54.5	8.8	49.0	44.0	58.3	60.1	46.6	48.3	46.3	57.0
X_{Ca}^{Gar}	.95		.24-.27	.88								.25

TABLE 4 (*continued*)

Phase	Cpx	Cpx	Cpx	Gar	Gar	Cpx	Cpx	Gar	Cpx	Gar	Glass	Glass	Gar
Run No	Z-19B	Z-19E	Z-19E	Z-19E	Z-19E	Z-22A	Z-22A	Z-22A	Z-22B	Z-22B	Z-22B	Z-22B	Z-22E
P Kbar/T°C	25/900	25/900	25/900	25/900	25/900	30/900	30/900	30/900	30/900	30/900	30/900	30/900	30/900
SiO_2	53.77	54.15	54.11	43.72	44.77	53.66	53.51	43.81	54.49	40.37	58.21	60.41	43.58
Al_2O_3	3.44	4.13	4.25	24.63	24.56	4.78	4.21	19.56	1.94	22.36	8.79	8.70	24.12
MgO	16.92	17.49	17.74	21.73	23.07	16.37	17.72	20.59	16.99	0.64	0.23	2.65	20.96
CaO	25.62	24.24	24.63	9.93	8.85	25.20	24.54	12.65	26.25	36.64	8.94	11.95	11.34
Total	99.75	100.01	100.73	100.01	101.25	100.01	99.98	96.61	99.67	100.01	76.17	83.71	100.00
Si	1.940	1.938	1.926	3.015	3.038	1.926	1.921	3.158	1.971	3.019	4.923	4.739	3.020
Al	0.146	0.174	0.178	2.002	1.965	0.202	0.178	1.662	0.083	1.971	0.876	0.805	1.970
Mg	0.910	0.933	0.941	2.234	2.333	0.876	0.948	2.212	0.916	0.071	0.029	0.310	2.165
Ca	0.990	0.930	0.939	0.732	0.643	0.969	0.944	0.977	1.018	2.935	0.811	1.005	0.842
Cation total	3.986	3.975	3.985	7.983	7.980	3.973	3.991	8.010	3.987	7.996	6.639	6.859	7.997
No. of oxygens	6	6	6	6	12	6	6	12	6	12	12	12	12
A	3.7	4.5	4.5	25.2	24.8	5.2	4.5	20.7	2.1	24.7	34.3	23.4	24.7
C	50.2	47.7	47.7	18.5	16.3	49.8	47.7	24.3	51.5	73.5	63.5	58.5	21.1
M	46.1	47.8	47.8	56.3	58.9	45.0	47.8	55.0	46.4	1.8	2.3	18.1	54.2
X_{Ca}^{Gar}				0.25	0.22			0.31		.95-.97			.24-.28

Phase	Glass	Cpx	Cpx	Zoisite	Glass	Glass	Cpx	Cpx	Glass	Cpx	Cpx	Tr	Tr
Run No	Z-22E	Z-23A	Z-23A	Z-23A	Z-23A	Z-23A	Z-24A	Z-24B	Z-24B	Z-24E	Z-24E	Z-24E	Z-24E
P Kbar/T°C	30/900	20/900	20/900	20/900	20/900	20/900	15/900	15/900	15/900	15/900	15/900	15/900	15/900
SiO_2	37.78	52.12	50.26	39.52	53.87	56.18	53.67	53.78	51.64	52.15	52.70	53.87	52.75
Al_2O_3	7.90	7.04	9.30	32.78	15.02	15.81	4.02	2.99	14.34	6.10	5.37	8.46	10.42
MgO	0.91	16.12	15.50	0.0	0.48	1.06	17.15	17.12	1.1	17.17	17.93	22.70	21.46
CaO	3.55	24.72	23.91	24.65	8.28	7.71	25.16	26.11	13.93	24.39	22.75	11.97	12.37
Total	50.14	100.00	98.97	96.95	77.64	80.76	100.00	100.00	81.01	99.81	98.75	97.00	97.00
Si	4.788	1.870	1.820	6.046	4.493	4.490	1.929	1.940	4.268	1.876	1.905	7.316	7.172
Al	1.180	0.298	0.397	5.911	1.476	1.490	0.170	0.127	1.397	0.259	0.229	1.355	1.670
Mg	0.172	0.862	0.836	0.000	0.059	0.126	0.919	0.921	0.135	0.920	0.996	4.594	4.348
Ca	0.482	0.950	0.928	4.041	0.740	0.660	0.969	1.009	1.233	0.940	0.881	1.742	1.802
Cation total	6.622	3.980	3.981	15.998	6.768	6.766	3.986	3.997	7.033	3.995	3.981	15.007	14.993
No. of oxygens	12	6	6	25	12	12	6	6	12	6	6	23	23
A	47.4	7.6	10.1	42.2	48.0	48.6	4.3	3.2	33.7	6.51	5.83	9.7	12.0
C	38.7	48.4	47.3	57.8	48.1	43.1	49.1	50.6	59.7	47.25	44.9	24.8	25.8
M	13.8	44.0	42.6	-	3.8	8.3	46.6	46.2	6.6	46.24	49.2	65.5	62.2
X_{Ca}^{Gar}													

TABLE 4 (*continued*)

Phase	Tr	Glass	Glass	Gar	Cpx	Tr	Tr	Tr	Cpx	Talc	Tr	Tr	Tr	Cpx
Run No	Z-24E	Z-24E	Z-24E	Z-27B	Z-27B	Z-27E	Z-27E	Z-27E	Z-27E	Z-27E	Z-28A	Z-28A	Z-28A	Z-28A
P Kbar/T°C	15/900	15/900	15/900	25/800	25/800	25/800	25/800	25/800	25/800	25/800	20/800	20/800	20/800	20/800
SiO_2	53.58	44.79	53.44	39.77	53.41	55.86	56.55	57.37	55.05	61.72	56.44	56.60	55.61	55.71
Al_2O_3	10.34	15.21	18.38	22.34	0.97	5.20	2.95	3.03	1.97	1.42	4.63	4.79	6.51	1.32
MgO	21.89	1.13	2.23	0.85	17.33	22.29	24.12	23.86	18.01	30.76	23.49	23.34	22.14	19.61
CaO	11.78	7.36	7.83	36.29	25.63	12.88	11.95	12.80	24.76	-	12.68	12.50	12.70	23.37
Total	97.59	68.49	81.88	99.25	97.34	96.24	95.57	97.06	99.79	93.91	97.24	97.23	96.96	100.01
Si	7.220	2.132	4.244	2.998	1.980	7.650	7.785	7.792	1.979	3.951	7.651	7.664	7.553	1.990
Al	1.643	0.853	1.721	1.985	0.042	0.840	0.479	0.484	0.083	0.107	0.740	0.765	1.042	0.055
Mg	4.396	0.080	0.263	0.096	0.958	4.550	4.948	4.828	0.965	2.936	4.746	4.710	4.482	1.044
Ca	1.701	0.375	0.666	2.931	1.018	1.891	1.763	1.862	0.953	-	1.842	1.814	1.848	0.894
Cation total	14.959	3.441	6.895	8.010	3.998	14.931	14.975	14.966	3.980	6.994	14.979	14.953	14.926	3.983
No. of oxygens	23	6	12	12	6	23	23	23	6	11	23	23	23	6
A	11.9	48.4	48.1	24.70	1.06	6.1	3.4	3.5	2.1	1.8	5.3	5.5	7.6	1.4
C	24.6	42.5	37.2	72.92	50.99	27.6	25.4	26.8	48.7	0.0	26.5	26.3	27.0	45.5
M	63.5	9.1	14.7	2.38	47.96	66.3	71.2	69.7	49.2	98.2	68.2	68.2	65.4	53.1
X_{Ca}^{Gar}				0.97										

Phase	Tr	Tr	Cpx	Cpx	Glass	Cpx	Cpx	Gar	Cpx	Tr	Tr	Glass
Run No	Z-29A	Z-29A	Z-29A	Z-29A	Z-29A	Z-29B	Z-30B	Z-30B	Z-30E	Z-34E	Z-34E	Z-34E
P Kbar/T°C	20/850	20/850	20/850	20/850	20/850	20/850	25/850	25/850	25/850	15/850	15/850	15/850
SiO_2	55.45	55.45	54.33	54.88	54.51	55.19	54.27	41.85	54.59	50.19	53.22	57.09
Al_2O_3	6.37	5.67	2.78	1.43	12.89	1.82	3.08	22.38	3.08	14.10	9.67	16.76
MgO	22.90	22.92	18.65	19.07	1.89	17.60	17.22	1.77	18.10	19.74	21.32	1.97
CaO	12.26	12.75	23.96	24.62	6.77	25.40	25.21	34.01	24.23	12.98	12.78	8.01
Total	96.98	96.79	99.72	100.00	76.06	100.01	99.78	100.01	100.00	97.01	96.99	83.83
Si	7.527	7.558	1.948	1.971	4.610	1.982	1.954	3.093	1.955	6.845	7.243	4.410
Al	1.019	0.911	0.118	0.060	1.285	0.077	0.130	1.950	0.130	2.267	1.551	1.526
Mg	4.633	4.656	0.997	1.021	0.238	0.942	0.923	0.195	0.966	4.012	4.324	0.227
Ca	1.783	1.862	0.920	0.947	0.614	0.978	0.971	2.694	0.930	1.897	1.864	0.663
Cation total	14.962	14.987	3.983	3.999	6.747	3.979	3.978	3.932	3.981	15.021	14.982	6.827
No. of oxygens	23	23	6	6	12	6	6	12	6	23	23	12
A	7.3	6.5	3.0	1.5	43.0	2.0	3.3	25.2	3.3	16.1	11.1	46.2
C	25.8	26.7	46.6	47.4	41.0	49.9	49.6	69.7	47.4	26.9	26.8	40.1
M	66.9	66.8	50.5	51.1	16.0	48.1	47.1	5.0	49.3	57.0	62.1	13.7
X_{Ca}^{Gar}								0.93				

TABLE 4 (*continued*)

Phase	Cpx	Tr	Gar	Tr	Cpx	Tr	Tr	Glass	Glass	Opx	Opx	Gar	Cpx
Run No	Z-38A	Z-38A	Z-38A	Z-38E	Z-39E	Z-39E	Z-39E	Z-39E	Z-39E	Z-44A	Z-44A	Z-44A	Z-44B
P Kbar/T°C	20/875	20/875	20/875	20/875	15/925	15/925	15/925	15/925	15/925	35/850	35/850	35/850	35/850
SiO_2	54.34	54.06	43.53	55.02	53.64	51.07	52.59	51.70	52.64	59.73	57.03	44.10	54.81
Al_2O_3	2.53	8.12	24.38	6.31	4.76	13.79	11.56	17.74	18.19	0.96	7.10	24.17	1.70
MgO	18.56	22.27	24.00	23.12	17.86	20.00	22.10	1.84	1.35	38.93	35.12	23.57	17.77
CaO	24.34	12.56	8.08	12.55	23.75	11.89	11.68	8.37	8.74	-	0.1	7.28	25.52
Total	99.77	97.01	99.99	97.00	100.01	96.76	97.93	79.65	80.92	99.62	99.66	99.12	99.80
Si	1.950	7.352	2.992	7.483	1.918	6.947	7.070	4.235	4.244	1.999	1.904	3.030	1.973
Al	0.107	1.302	1.975	1.012	0.201	2.212	1.832	1.713	1.729	0.038	0.279	1.957	0.072
Mg	0.993	4.514	2.459	4.686	0.952	4.055	4.428	0.225	0.162	1.939	1.748	2.413	0.953
Ca	0.936	1.830	0.595	1.829	0.910	1.733	1.683	0.735	0.755	-	0.015	0.536	0.984
Cation total	3.986	14.998	8.021	15.011	3.981	14.947	15.013	6.908	6.891	3.976	3.946	7.936	3.982
No. of oxygens	6	23	12	23	6	23	23	12	12	6	6	12	6
A	2.7	9.3	24.4	7.2	5.1	16.0	13.0	47.1	48.5	1.0	7.3	24.9	1.8
C	47.2	26.2	14.7	26.0	46.4	25.1	23.9	40.5	42.4	-	0.8	13.6	49.9
M	50.1	64.5	60.8	66.8	48.5	58.9	63.0	12.4	9.1	99.0	91.9	61.4	48.3
X_{Ca}^{Gar}			0.19									0.18	

Phase	Cpx	Cpx	Gar	Cpx	Glass	Grt	Grt	Cpx	Cpx	Glass	Opx
Run No	Z-44B	Z-44E	T-980	T-980	T-981	T-981	T-1023	T-1055	T-1055	T-1055	T-1201
P Kbar/T°C	35/850	35/850	30/1000	30/1000	25/850	25/850	35/900	35/900	35/900	35/900	15/950
SiO_2	55.08	54.95	43.99	53.51	63.22	44.14	44.01	54.46	55.15	57.33	56.18
Al_2O_3	2.30	2.59	24.13	6.73	12.47	24.33	24.25	4.81	2.99	9.33	6.58
MgO	17.37	18.03	22.38	16.1	1.08	22.24	22.37	24.02	24.06	n.d.	36.71
CaO	25.25	24.42	9.50	23.66	5.99	9.3	9.38	16.71	17.58	6.30	0.53
Total	100.00	99.99	100.0	100.0	82.8	100.01	100.01	100.01	99.78	72.96	100.0
Si	1.977	1.968	3.031	1.908	4.847	3.037	3.030	1.944	1.972	4.968	1.880
Al	0.097	0.109	1.959	0.283	1.127	1.973	1.968	0.202	0.126	0.957	0.260
Mg	0.930	0.963	2.298	0.856	0.123	2.281	2.296	0.919	0.922	n.d.	1.831
Ca	0.971	0.937	0.701	0.904	0.492	0.685	0.692	0.889	0.937	0.593	0.019
Cation total	3.975	3.977	7.989	3.951	6.589	7.976	7.986	3.954	3.962	6.336	3.990
No. of oxygens	6	6	12	6	12	12	12	6	6	12	6
A	2.5	2.8	24.6	7.4	47.8	25.0	24.8	5.3	3.3	44.66	6.6
C	49.8	47.9	17.62	47.5	41.7	17.3	17.4	46.6	48.7	55.34	0.96
M	47.7	49.3	57.76	45.0	10.5	57.7	57.8	48.1	48.0	-	92.5
X_{Ca}^{Gar}			23.4			23.1	23.16				

TABLE 4 (*continued*)

Phase	Cpx	Cpx	Glass	Glass	Cpx	Cpx	Opx	Opx	Gar	Cpx	Opx	Glass	Grt	Cpx	Opx
Run No	T-1201	T-1201	T-1201	T-1201	T-1201	T-1201	T-1201	T-1201	T-1203	T-1203	T-1203	T-1203	T-1204	T-1204	T-1204
P Kbar/T°C	15/950	15/950	15/950	15/950	15/950	15/950	15/950	15/950	15/950	15/950	15/950	15/950	27/850	27/850	27/850
SiO_2	53.46	54.67	64.71	63.04	54.86	53.34	56.3	58.72	43.45	56.29	58.89	77.84	43.60	55.85	57.86
Al_2O_3	4.69	2.38	23.33	23.2	2.68	4.61	6.65	2.50	25.10	3.48	3.61	14.25	25.11	2.59	4.54
MgO	18.06	19.14	1.55	3.24	19.06	18.47	36.53	37.89	22.43	16.78	37.27	0.71	23.28	17.82	36.52
CaO	23.50	23.54	10.22	10.53	23.28	23.27	0.52	0.89	9.02	23.28	0.23	7.05	8.00	23.55	1.08
Total	99.71	99.73	83.87	81.89	99.85	99.69	100.0	100.0	99.9	99.83	100.0	76.42	99.99	99.81	100.0
Si	1.913	1.957	4.222	4.129	1.960	1.909	1.883	1.965	2.990	1.999	1.963	4.927	2.992	1.991	1.936
Al	0.198	0.100	1.794	1.791	0.113	0.194	0.262	0.099	2.036	0.146	0.142	1.063	2.031	0.109	0.179
Mg	0.964	1.021	0.151	0.316	1.015	0.985	1.822	1.890	2.301	0.888	1.852	0.067	2.381	0.947	1.821
Ca	0.901	0.903	0.714	0.739	0.891	0.892	0.018	0.032	0.665	0.886	0.008	0.478	0.588	0.899	0.039
Cation total	3.986	3.980	6.881	6.975	3.982	3.980	3.986	3.986	7.992	3.92	3.965	6.535	7.992	3.952	3.975
No. of oxygens	6	6	12	12	6	6	6	6	12	6	6	12	12	6	6
A	5.04	2.55	50.89	45.91	2.9	4.9	6.6	2.5	25.5	3.9	3.6	49.36	25.5	2.9	4.6
C	45.9	45.73	40.53	37.88	45.4	45.2	0.9	1.6	16.7	48.0	0.4	44.4	14.7	47.3	2.0
M	49.1	51.73	8.57	16.22	51.7	49.9	92.4	95.9	57.7	48.1	95.8	6.23	59.8	49.8	93.4
X_{Ca}^{Gar}									22.4				20.0		

Phase	Glass	Tr	Tr	Glass	Gar	Cpx	Opx	Glass	Gar	Cpx	Opx
Run No	T-1204	T-1244	T-1396	T-1402	T-1402	T-1402	T-1402	T-1405	T-1405	T-1405	T-1405
P Kbar/T°C	27/850	17/850	17/850	23/950	23/950	23/950	23/950	23/925	23/925	23/925	23/925
SiO_2	78.82	54.66	54.95	73.34	44.04	53.65	57.49	74.37	43.75	53.84	57.76
Al_2O_3	13.7	11.30	9.45	17.08	24.42	5.06	5.44	16.78	24.95	5.47	5.82
MgO	0.52	21.27	22.31	2.08	24.18	17.92	36.47	1.90	24.14	18.57	35.66
CaO	6.81	12.68	13.29	7.50	7.36	23.37	0.61	6.96	7.16	22.12	0.76
Total	82.0	99.91	100.00	82.81	100.0	100.0	100.01	82.62	100.0	100.0	100.0
Si	4.978	7.201	7.259	4.681	3.017	1.916	1.920	4.730	2.996	1.915	1.928
Al	1.019	1.754	1.472	1.285	1.971	0.213	0.214	1.258	2.013	0.229	0.230
Mg	0.049	4.177	4.392	0.198	2.469	0.954	1.816	0.180	2.464	0.984	1.774
Ca	0.461	1.790	1.881	0.513	0.540	0.894	0.022	0.474	0.526	0.843	0.027
Cation total	6.507	14.922	15.004	6.677	7.997	3.977	3.972	6.682	7.999	3.971	3.959
No. of oxygens	12	23	23	12	12	6	6	12	12	6	6
A	50.0	12.81	10.5	47.49	24.67	5.45	5.5	49.0	25.18	5.90	6.0
C	45.2	26.15	26.84	37.89	13.52	45.74	1.13	36.9	13.16	43.42	1.41
M	4.8	61.03	62.66	14.61	61.81	48.81	93.37	14.1	61.65	50.68	92.59
X_{Ca}^{Gar}									17.6		

TABLE 4
(continued)

Phase	Glass	Gar	Cpx	Opx	Gar	Cpx	Opx	Glass
Run No	T-1416	T-1416	T-1416	T-1416	T-1445	T-1445	T-1445	T-1445
P Kbar/T°C	23/900	23/900	23/900	23/900	23/875	23/875	23/875	23/875
SiO_2	74.16	44.02	54.68	56.45	43.57	54.87	56.33	72.92
Al_2O_3	15.85	24.84	2.94	7.84	24.95	4.53	7.29	16.67
MgO	2.23	23.97	18.46	35.14	23.25	17.61	36.07	2.74
CaO	7.77	7.17	23.93	0.57	8.24	22.99	0.31	7.67
Total	77.61	100.00	100.01	100.0	100.01	100.00	100.00	78.64
Si	4.734	3.012	1.956	1.884	2.992	1.952	1.881	4.664
Al	1.192	2.003	0.124	0.308	2.019	1.190	0.287	1.257
Mg	0.212	2.444	0.984	1.748	2.380	0.934	1.796	0.261
Ca	0.531	0.526	0.917	0.020	0.606	0.877	0.011	0.526
Cation total	6.669	7.985	3.981	3.960	7.997	4.953	3.975	6.708
No. of oxygens	12	12	6	6	12	-6	-6	-12
A	44.5	25.22	3.16	8.01	25.27	4.98	7.36	44.4
C	39.7	13.24	46.71	1.04	15.17	46.01	0.56	37.16
F	15.8	61.54	50.13	90.9	59.57	49.00	92.08	18.4
X_{Ca}^{Gt}		17.7			20.3			

different thermodynamic data bases (app. 2), the assemblage Tal + Zoi + Qtz is not stable in the vicinity of the H_2O-saturated solidus (figs. A-1A,B, and C) in contrast to the suggestion by Ellis and Thompson (1986, fig. 9). The stable coexistence of this assemblage is important as it is a higher pressure hydrous equivalent of Anr + Opx. Coexisting idiomorphic zoisite and talc have been reported from the metamorphosed Allalin Gabbro, Switzerland, which also contains kyanite-eclogite assemblages (Chinner and Dixon, 1973).

In CMASH as in CASH (Boettcher, 1970), the H_2O-saturated solidus for zoisite-bearing assemblages has a positive dP/dT reflecting the higher

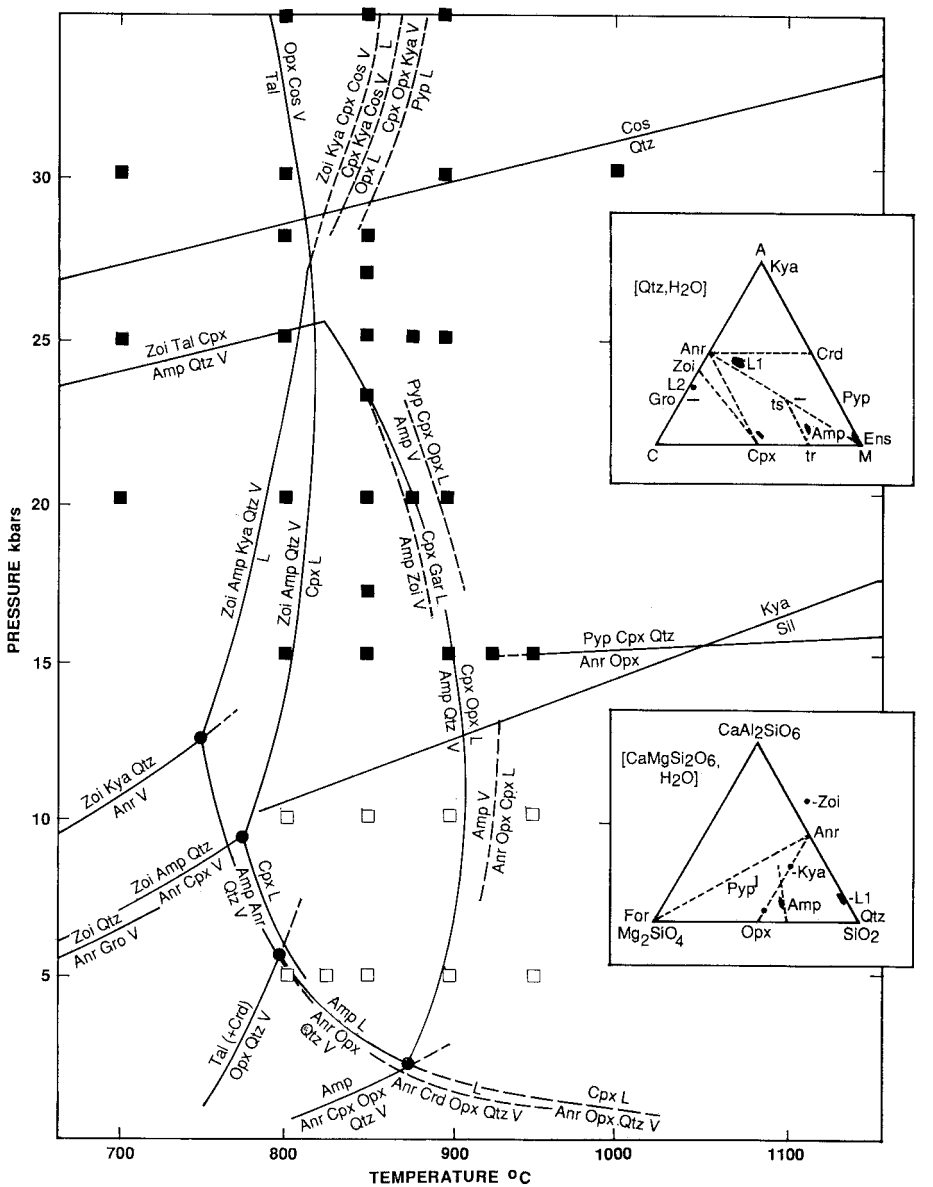

Fig. 3. Pressure-temperature diagram showing the location of key melting and subsolidus reactions from the CMASH experiments with excess quartz and H_2O. Filled squares represent experimental data points presented in table 3. The reaction limiting the stability of Amp + Qtz + H_2O (9) does not involve Anr nor Gar and thus backbends due to phase compressibility not because of a phase change. Around 25 kb in the subsolidus region Amp + Qtz + H_2O is replaced by Zoi + Tal + Cpx. At the H_2O-saturated solidus from about 12 to 25 kb, the melts are always peraluminous. The main difference from Ellis and Thompson (1986, fig. 5, reaction 18) is the relocation of this reaction involving Zoi + Tal + Qtz to much higher pressures and lower temperatures so as not to intersect the H_2O-saturated solidus.

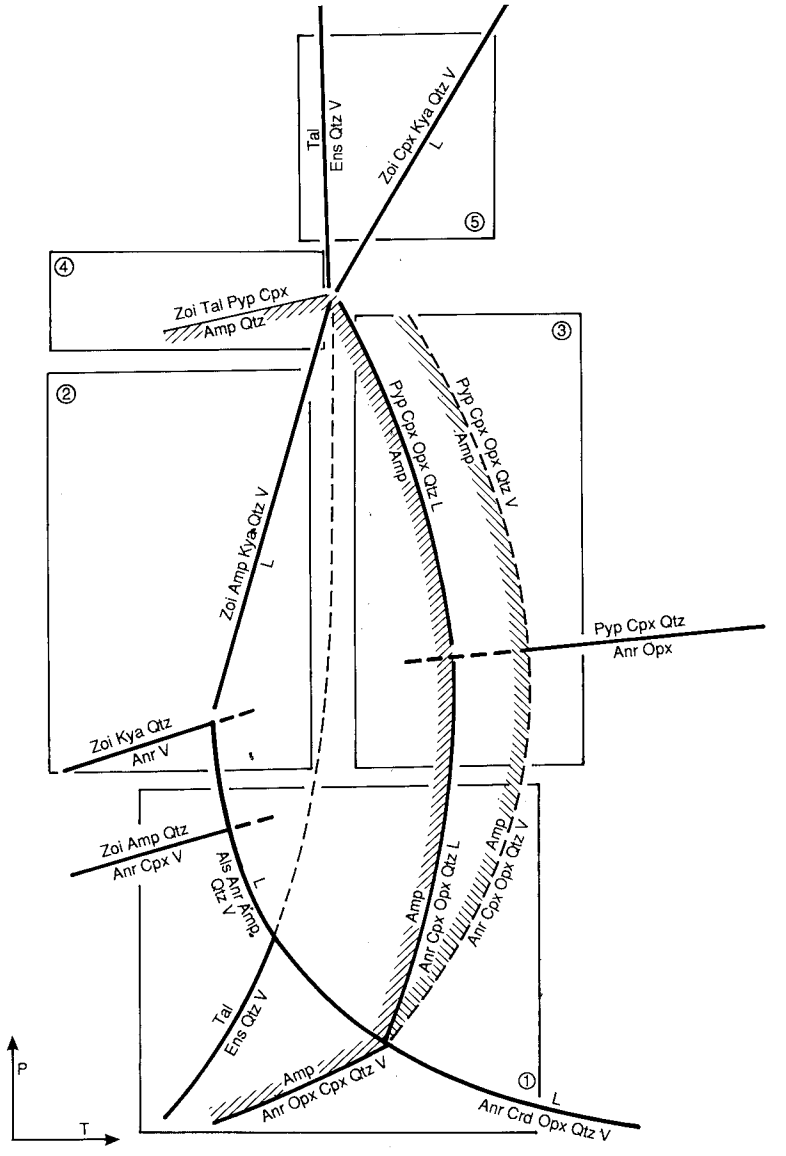

Fig. 4. Schematic P-T diagram showing how petrogenetic grids constructed entirely from dehydration and solid-solid reactions (even though metastable) bracket the hydrous melt region. The change of dP/dT at the H_2O-saturated solidus (from negative to positive) results mainly from the change in density of the subsolidus assemblage with the removal of plagioclase. The backbending of amphibole dehydration (metastable dashed line through regions 1 and 3) and dehydration-melting reflects the density change occurring as plagioclase assemblages are replaced by garnet-bearing ones and also due to the compressibility of amphibole and melt. The numbered boxed regions are used to orient the discussions in the text.

density of such assemblages compared to those with anorthite. The lowest temperature H_2O-saturated solidus for mafic compositions in CMASH between about 12 and 18 to 25 kb (fig. 3 and region 2 in fig. 4) appears to be defined by the reaction

$$\text{Zoi} + \text{Amp} + \text{Kya} + \text{Qtz} + \text{V} = \text{L} \quad (6)$$

Near 25 kb the nature of the solidus reaction depends upon the relative subsolidus stability of Zoi + Amp or Amp + Kya (see app. 2). Figure 5 shows the schematics of phase relations with quartz- and H_2O-saturated reaction topologies deduced for this P-T region in CMASH for the two cases A and B outlined in appendix 2. For case (A) Amp + Kya dehydrates at lower P-T than Zoi + Amp (fig. A-1A and inset in fig. 5), and case (B) is the reverse (Amp + Kya dehydrates at higher P-T than Zoi + Amp, see fig. A-1C and main figure in fig. 5). For case A (inset A, fig. 5), the sequential H_2O-saturated solidus reactions at pressures higher than 25 kb are (6) followed by

$$\text{Zoi} + \text{Pyp} + \text{Kya} + \text{Qtz} + \text{V} = \text{L} \quad (7)$$

For case B (main part of fig. 5), they are reaction (6) followed by

$$\text{Zoi} + \text{Cpx} + \text{Kya} + \text{Qtz} + \text{V} = \text{L} \quad (8)$$

then possibly by reaction (7), see box at top right of figure 5.

Reaction (6) represents the melting of epidote-amphibolites (in CMASH, with excess H_2O), from about 10 to near 25 kb, and occurs between 800° and 850°C (fig. 3). Near 25 kb, H_2O-saturated melting appears to occur first in epidote-eclogites (Zoi + Cpx + Pyp + Qtz) or in zopydites (Zoi + Cpx + Kya(Disthen) + Qtz) rather than in amphibolites.

In the region near 25 kb and 800°C (figs. 3, 4, and 5) a complex series of invariant points must occur because of the convergence of reactions, also including Tal and Opx. The exact resolution of these invariant points is not easily determined from available experiments, but the experimental results in CMASH (table 3) appear to favor case B at these pressures (see figs. 3 and 5).

The upper thermal stability of amphibole ± quartz with excess H_2O from 15 to 25 kb.—The reaction marking the upper limit of Amp + Qtz + V stability in CMASH (region 3 in fig. 4) is a melting reaction apparently without anorthite or garnet (see fig. 3), that is

$$\text{Amp} + \text{Qtz} + \text{V} = \text{Cpx} + \text{Opx} + \text{L} \quad (9)$$

This reaction was located at 5 and 10 kb by Ellis and Thompson (1986, fig. 5, p. 105), and at higher pressures it must pass below 23 kb 850°C (run T-1439), and it therefore shows a change from positive to negative dP/dT in the 15 kb region (figs. 3 and 4). Because this reaction does not involve anorthite or garnet in this region, the backbending cannot reflect

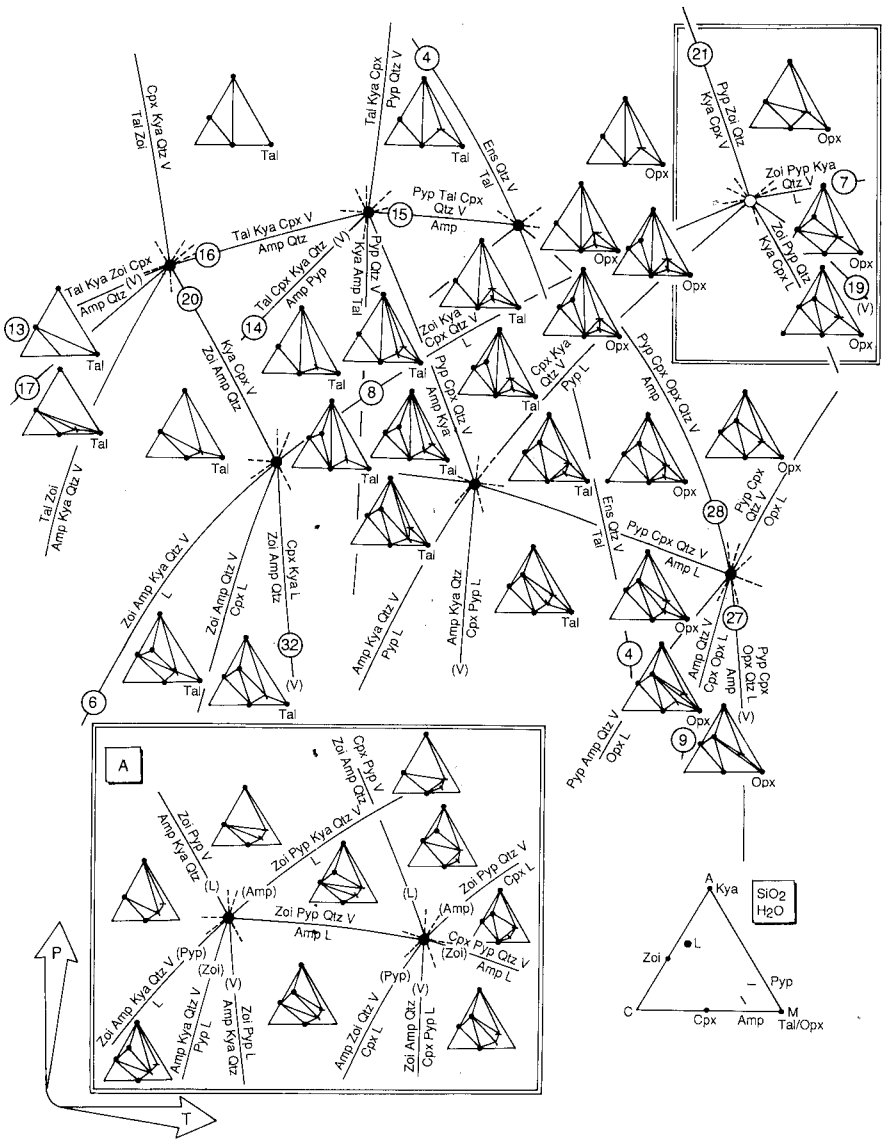

Fig. 5. Schematic P-T diagrams showing the detailed interpretation of quartz- and H_2O-saturated experiments close to the H_2O-saturated solidus in CMASH from about 15 to 35 kb. The topologies illustrated in the main figure (Zoi + Amp dehydration occurring at slightly lower P-T conditions than the Amp + Kya dehydrations) correspond to case B. The inset shows case A, where these reactions are reversed, as discussed in app. 2. The key-diagram in the lower right identifies the phases involved. The boxed region in the upper right shows the unusual phase relations involving Kya, Cpx, Pyp, Zoi, Qtz, V, and L. The numbered reactions are those in table 2. Two-phase bundles of tie lines are represented by individual lines. Quartz-absent reactions are not presented. The P-T extent of the H_2O(V)-absent reactions is not known. No attempt has been made to locate geometrically metastable invariant points. Some reactions are written with quartz, even though coesite may be the stable polymorph.

a phase change and must be due to the relative compressibilities of H_2O, melt, and amphibole.

Two other melting-reactions involving amphibole, but without quartz, were approximately located in figure 3 (see table 3 and fig. 2B);

$$\text{Amp} + \text{V} = \text{Pyp} + \text{Cpx} + \text{Opx} + \text{L} \tag{10}$$

and

$$\text{Amp} + \text{Zoi} + \text{V} = \text{Pyp} + \text{Cpx} + \text{L} \tag{11}$$

The sub-solidus disappearance of amphibole + quartz near 25 kb (a model for the disappearance of amphibole in eclogites).—As noted in figure 1B, the upper pressure stability limit of tremolite in CMSH is determined by the H_2O-conserving reaction (J. B. Thompson, 1981, 1982)

$$Ca_2Mg_5SiO_{22}(OH)_2[\text{Tre}] = 2CaMgSi_2O_6[\text{Dio}] + Mg_3Si_4O_{10}(OH)_2[\text{Tal}] \tag{5}$$

This reaction becomes continuous in CMASH, with $Al_2Mg_{-1}Si_{-1}$ being greater in Amp than Cpx, with very little alumina going into talc. Because the three hydrous minerals (Amp, Zoi, and Tal) are stable over a large P-T range, several H_2O-conserving reactions are possible (region 4 in fig. 4). Their form may be deduced with the help of figure 6, which shows the plane $CaAl_2Si_2O_8$(Anr)–$MgSiO_3$(Ens)–H_2O projected from $CaMgSi_2O_6$ + SiO_2 (quartz) and is most useful for depicting reactions in the fluid-absent region for mafic compositions. The upper pressure stability of Amp + Qtz in CMASH could theoretically be defined by one or more of the H_2O-conserving reactions:

$$\text{Zoi} + \text{Tal} + \text{Pyp} + \text{Cpx} = \text{Amp} + \text{Qtz} \tag{12}$$

$$\text{Zoi} + \text{Tal} + \text{Kya} + \text{Cpx} = \text{Amp} + \text{Qtz} \tag{13}$$

$$\text{Cpx} + \text{Tal} + \text{Kya} = \text{Amp} + \text{Qtz} + \text{Pyp} \tag{14}$$

It is suggested in figure 7 for case B that the upper-pressure stability limit of Amp + Qtz consists of several reaction segments. These include two dehydration reactions

$$\text{Amp} = \text{Pyp} + \text{Tal} + \text{Cpx} + \text{Qtz} + \text{V} \tag{15}$$

$$\text{Amp} + \text{Qtz} = \text{Tal} + \text{Kya} + \text{Cpx} + \text{V} \tag{16}$$

plus the H_2O-conserving reaction (13). Note that quartz changes from product to reactant along these segments.

The experimental data (tables A-1, -3, -4 and fig. 3) indicate that the high pressure stability of Amp + Qtz in CMASH is represented by dehydration reactions occurring near 25 kb, for example,

$$\text{Tal} + \text{Cpx} + \text{Zoi} = \text{Amp} + \text{Qtz} + \text{V} \tag{17}$$

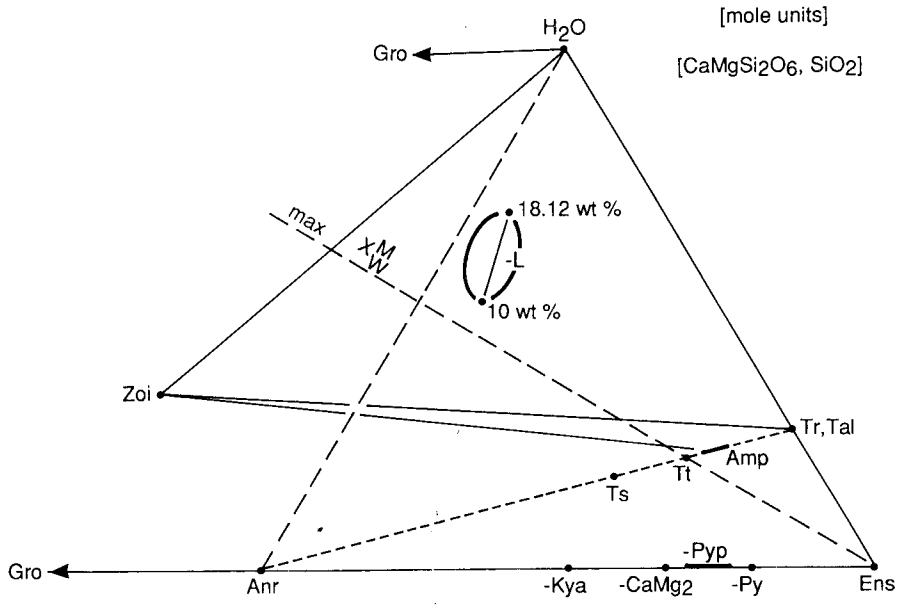

Fig. 6. Molar projections from $CaMgSi_2O_6$ and SiO_2 onto $CaAl_2Si_2O_8$(Anr) + $MgSiO_3$(Ens) + H_2O in CMASH permit the representation of the water-deficient region. The melts (labelled-L) lie below the plane as they are corundum normative. It is possible to examine all possible water-conserving reactions involving two or more hydrous minerals or one hydrous mineral and H_2O-undersaturated melt. The dashed line labelled "max X_w^m" constructed between the most aluminous amphibole observed (fig. 2) and Ens (in projection from Cpx, Qtz) shows the boundary for H_2O undersaturated melts consistent with the proposition that dehydration-melts are always more hydrous than the hydrous phases breaking down.

with H_2O as part of the low-pressure assemblage and reaction (15) with H_2O on the high pressure side. These are related to reaction (13) in figure 7. It will be noted in figure A-1A and B that the two thermodynamic data bases give subsolidus Amp-out reactions that are almost 10 kb apart and differ because of the calculated relative positions of Zoi + Amp and Amp + Kya reactions.

Near-solidus (H_2O-saturated) phase relations in the range 25 kb to 35 kb (a model for the generation of arc magmas).—Because of the convergence of the wet solidus and the disappearance of Amp + Qtz and of talc near 800°C and about 30 kb, many reactions are compressed into a small P-T region. This P-T region is important for the generation of arc magmas (Gill 1981; Drummond and Defant, 1990; Peacock, Rushmer, and Thompson, 1994). At pressures higher than the disappearance of amphibole (~26 kb) and at temperatures higher than the dehydration of talc (region 5 in fig. 4), the system CMASH serves as a model for zoisite-bearing coesite eclogites. Sekine, Wyllie, and Baker (1981, p. 943) report the H_2O-saturated

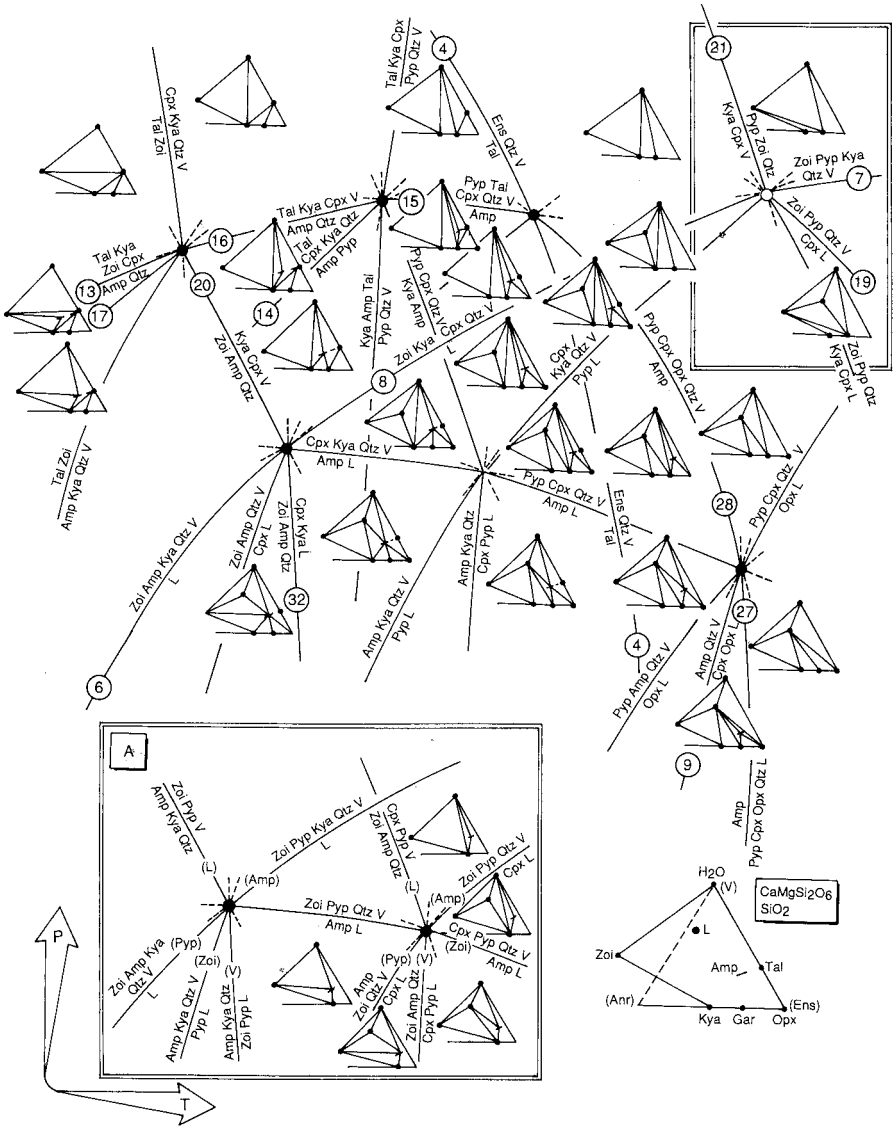

Fig. 7. Projections including fluid-absent reactions onto $CaAl_2Si_2O_8 + MgSiO_3 + H_2O$ (from $CaMgSi_2O_6$, SiO_2; fig. 6) superimposed onto petrogenetic grids for case B. These show the principal reactions that govern the evolution of CMASH melts in the H_2O-undersaturated region. The inset shows case A. This diagram is the same form as figure 5—see caption.

solidus reaction

$$\text{Cpx} + \text{Pyp} + \text{Cos} + \text{Zoi} + \text{V} = \text{L} \quad (18)$$

to define eutectic melting in CMASH at 30 kb between 800° to 825°C. However, the liquids produced are peraluminous which would rather indicate the peritectic reaction

$$\text{Zoi} + \text{Pyp} + \text{Cos} + \text{V} = \text{Cpx} + \text{L} \quad (19)$$

Eutectic melting of Zoi + Pyp + Cpx + Qtz + V would produce definitely sub-aluminous liquids.

Our experimental results (table 3, fig. 3) suggest that the subsolidus dehydration reaction

$$\text{Zoi} + \text{Amp} + \text{Cos} = \text{Cpx} + \text{Kya} + \text{V} \quad (20)$$

has occurred by 800°C, at 30 and 35 kb. Unfortunately there are insufficient data to locate the reaction

$$\text{Zoi} + \text{Pyp} + \text{Cos} = \text{Cpx} + \text{Kya} + \text{H}_2\text{O} \quad (21)$$

which has taken place in this P-T range (but see the inset in the top-right of fig. 7). The thermodynamic calculations have introduced even further complications regarding this reaction (see app. 2).

The H_2O-saturated solidus at 30 to 35 kb for case B would be represented by reaction (8) with coesite instead of quartz but would not occur in many eclogite compositions in CMASH. The equivalent H_2O-saturated solidus for case A would be represented by reaction (7) with coesite instead of quartz.

We have not observed the certain coexistence of Zoi + Pyp with quartz and H_2O in our experiments, although Sekine, Wyllie, and Baker (1981, p. 942) report it at 30 kb in their model quartz-eclogite experiments. The assemblage Zoi + Pyp + Qtz was found only in those experiments of Sekine, Wyllie, and Baker (1981) initially held at much higher temperatures where melting occurs and garnet is stable, then dropped to lower temperatures. It is possible that large garnets formed at high T in these experiments persisted metastably to lower temperatures simply because of their size and therefore were not in equilibrium with Zoi + Qtz + V below the solidus.

Our experimental results (table 3) imply further that at temperatures higher than the dehydration of talc (fig. 3), the H_2O-saturated solidus for a large range of mafic compositions is described by the peritectic reactions

$$\text{Cpx} + \text{Kya} + \text{Qtz} + \text{V} = \text{Opx} + \text{L} \quad (22)$$

and in quartz-absent compositions (requiring the breaking of Cpx-Pyp tie lines) by

$$\text{Cpx} + \text{Opx} + \text{Kya} + \text{V} = \text{Pyp} + \text{L} \quad (23).$$

The present experiments are insufficient to decide whether case A or case B (fig. 5) is more appropriate for CMASH. Sekine, Wyllie, and Baker (1981, p. 947) consider that while zoisite may be the relevant subsolidus mineral at 30 to 35 kb in CMASH (our case B), kyanite (Stern and Wyllie, 1978, p. 646) is likely to be the subsolidus mineral in gabbro (our case A). Furthermore the CMASH system does not include solid solutions involving Na (pyroxene) and Fe (pyroxene, garnet). Recent experiments at ETH Zürich have included these components in natural compositions (tonalite: Schmidt, 1993; MORB: Poli, 1993) and leads to the conclusion (Poli and Schmidt, 1993; Schmidt and Thompson, 1993) that lawsonite replaces zoisite near 25 kb at any solidus appropriate to basaltic and intermediate-rock compositions. In addition even in CMASH other hydrous phases (such as Mg-Al pumpellyite, for example, Schreyer, 1988; chloritoid, Poli, 1993) are likely to be stable close to the H_2O-saturated solidus at pressures greater than 35 kb. Future experiments relevant to dehydration of deep subducted slabs will determine how the H_2O-saturated basalt solidus continues to increase in temperature above 35 kb.

Phase relations in the grossular-rich part of the CMASH system.—Experiments in the Ca-rich part of the CMASH system (molar CaO richer than Zoi + Cpx, fig. 2A) were carried out using glass B (tables A1, 3). In contrast to the Mg-rich part of the system, phase relations involving grossular-rich garnet are much simpler to describe. Only three subsolidus assemblages involve grossular-rich garnet (Gro) up to 35 kb, Gro + Cpx + Anr + Qtz + V as well as Gro + Zoi + Anr + Qtz + V at low pressures (see Ellis and Thompson, 1986) and Gro + Cpx + Zoi + Qtz + V at higher pressures.

Melting occurs at a lower temperature in grossular-rich regions than in the more Mg-rich assemblages with the initial melting being defined by two eutectic reactions

$$\text{Gro} + \text{Cpx} + \text{Anr} + \text{Qtz} + \text{V} = \text{L} \tag{24}$$

and

$$\text{Gro} + \text{Cpx} + \text{Zoi} + \text{Qtz} + \text{V} = \text{L} \tag{25}$$

The Cpx + Anr + Qtz + V and Cpx + Zoi + Qtz + V assemblages (at lower and higher pressures, respectively) represent thermal divides separating these per-calcic, sub-aluminous liquids from the met- or per-aluminous initial liquids of the Mg-richer part of the system (fig. 2A). The grossular-rich garnet (Gro) shows little change in composition toward pyrope over the entire P-T range studied. Liquid compositions are more Ca-rich than the Cpx-Zoi tie-line on an ACM diagram (L2 in fig. 2A).

As can also be seen in table 3 and figure 2A, the assemblage Cpx + Zoi + Gro + Qtz + H_2O melted eutectically to give a percalcic liquid (L2) from 15 to 35 kb (fig. 2A). Thus under H_2O- and quartz-excess conditions grospydites (Gro + Cpx + Kya ± Qtz) cannot form in CMASH, being

represented instead by Zoi + Cpx + Kya + Qtz/Cos coexisting with model kyanite eclogites with Cpx + Pyp + Kya + Qtz/Cos.

THE DISAPPEARANCE OF QUARTZ IN WATER-SATURATED MELTS FROM CMASH AMPHIBOLITES

At water saturation, the initial melts are very siliceous (fig. 2B), removing quartz from most amphibolites during melt generation. As with other peritectic systems (A. B. Thompson, 1982; Ellis and Thompson, 1986), water-saturated melting of mafic compositions is distinguished from dehydration-melting by the persistence of quartz to higher temperatures in the latter.

Many of the experiments, even though starting with quartz well in excess of that normally found in amphibolites, lost quartz at or just above water-saturated melting. This occurs because the melts are all very siliceous (compare the Anr + Qtz + H_2O eutectic compositions with the melt compositions projected from $CaMgSi_2O_6$ and H_2O in figure 2B).

As can also be seen in figure 2B, the melt compositions become slightly less siliceous from 5 to 15 kb, presumably reflecting net-transfer reactions with Anr + Qtz and Cpx or Amp. After the disappearance of Anr the melt compositions become progressively more siliceous (20-30 kb), as the production of garnet releases SiO_2 through net transfer reactions with Gar + Cpx or Opx.

At pressures above about 25 kb and at temperatures above Amp + Qtz breakdown, Gar + Cpx + Zoi + Qtz (or Cos) in CMASH coexisted with H_2O-saturated peraluminous liquids (as also observed by Sekine, Wyllie, and Baker 1981, at 30 kb), although in the bulk compositions used by us, quartz had disappeared at these conditions with excess H_2O.

DEHYDRATION MELTING AND AMPHIBOLE DISAPPEARANCE IN CMASH

Because the melting relations discussed so far, and indeed most of the experiments conducted, apply to the water-excess region, it is necessary to consider where, in P-T space, melting will occur if water is not present in excess (that is, only available from breakdown of hydrous minerals). With regard to the schematic isobaric T-X section between anhydrous phases (An), an hydrous mineral (H), and H_2O (V) shown in the lower right inset in figure 8, the lowest temperature melts would be produced at water saturation through the simplified reaction H + V = L at point Eu (fig. 8).

Because amphibole (without excess fluid) always persists to higher temperatures than water-saturated melting up to its disappearance near 25 kb PH_2O, it is inferred that the melting reactions of Amp are always peritectic to anhydrous minerals and a water-undersaturated melt containing more dissolved H_2O than Amp. With regard to the simple model binary system An-H_2O (fig. 8 inset), the lowest temperature reaction is always H + V = L followed by H = An + L. This would mean that Amp never melts congruently and that the generalized eutectic reaction H + An = L is never achieved for amphibole (Eggler, 1973, 1978).

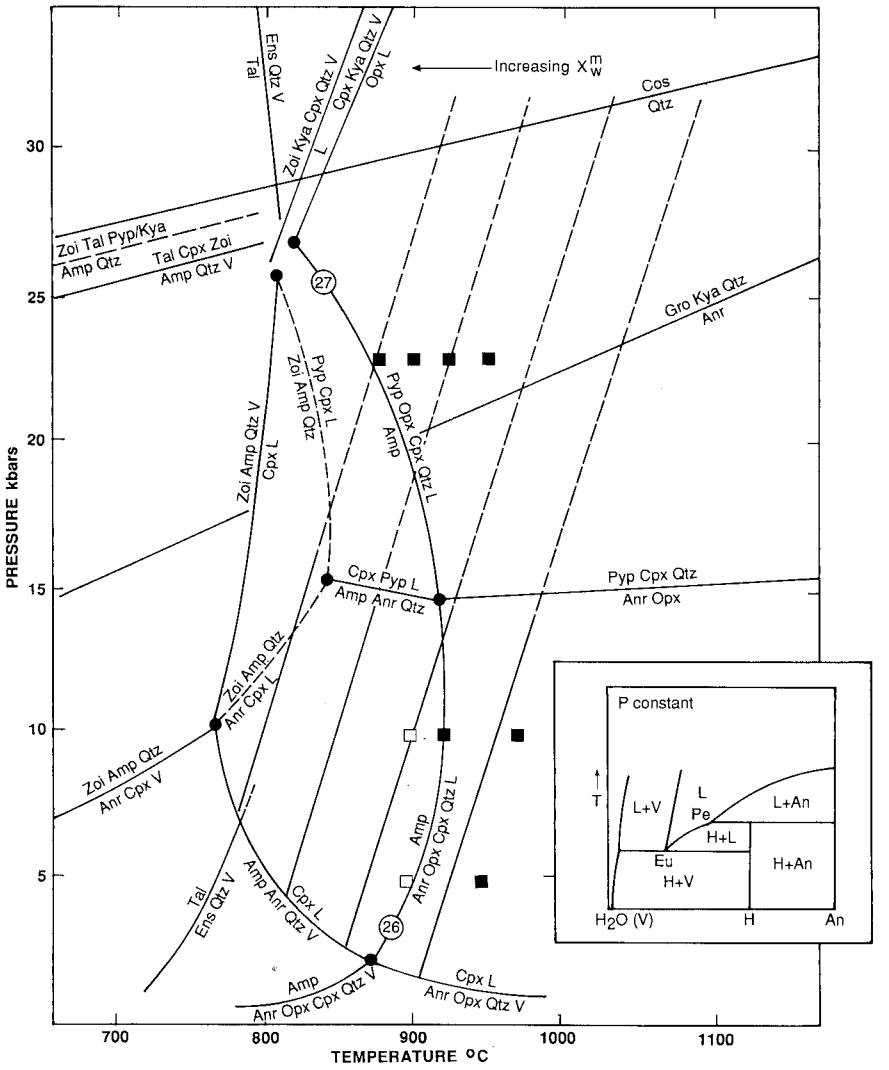

Fig. 8. Pressure-temperature diagram showing possible configurations of water-conserving (fluid-absent) reactions relevant to the disappearance of amphibole at quartz-saturation in CMASH. The lower pressure region shows the dehydration-melting reaction Amp = Anr + Cpx + Opx + Qtz + L (26) barely cutting the X_w^m (constant mole fraction of H_2O in the melt) contours as proposed by Burnham (1979). The high pressure dehydration-melting reaction Amp = Pyp + Cpx + Opx + Qtz + L (27) distinctly cuts the X_w^m contours, resulting in a continuous decrease in the amount of melt produced with increasing pressure in the direction of the H_2O-saturated solidus. The location of the dehydration-melting reactions involving Zoi + Amp + Qtz (shown by dashed lines) are not well constrained.

On the basis of available data, we cannot exclude the possibility that at low pressures (<3 kb) the tie line Amp-Opx (in projection from $CaMgSi_2O_6$, SiO_2, fig. 6) can act as a thermal barrier. By analogy with experiments on phlogopite (Yoder and Kushiro, 1969) it has been proposed (Eggler, 1978; Burnham, 1979a) that some melts produced from amphibolite can have less H_2O than coexisting amphiboles (see also Grant, 1986; Vielzeuf and Clemens, 1993). According to the possibility advanced in the inset diagrams in figure 7, any proportions of H and V would yield eutectic melts at water saturation. For initial proportions of V less than Eu, the melt would become water-undersaturated with further increase in temperature. Most experimental investigations of the water-undersaturated region (D. H. Green, 1973; Sekine, Wyllie, and Baker 1981; Ellis and Thompson, 1986, Rushmer, 1991) consider compositions between An and H. We will attempt to consider theoretically the water deficient region of CMASH and reactions of the type H = An + L at the simplified peritectic (Pe, inset in fig. 8) in the model system.

Ellis and Thompson (1986 fig. 4) deduced that the dehydration-melting reaction removing Amp from quartz saturated liquids in CMASH at pressures below about 15 kb, was

$$\text{Amp} = \text{Anr} + \text{Opx} + \text{Cpx} + \text{Qtz} + \text{L} \qquad (26)$$

This fluid-absent amphibolite solidus lies between 900° to 925°C at 10 kb, and between 900° to 950°C at 5 kb (Ellis and Thompson, 1986, p. 113, open and solid squares in fig. 8). At the intersection with the reaction

$$\text{Anr} + \text{Opx} = \text{Pyp} + \text{Cpx} + \text{Qtz} \qquad (1)$$

reaction (26) would presumably then become

$$\text{Amp} = \text{Pyp} + \text{Cpx} + \text{Opx} + \text{Qtz} + \text{L} \qquad (27)$$

from about 15 to 25 kb, even if amphiboles were as aluminous as $tr_{30}ts_{70}$ (see fig. 6).

These breakdown reactions for amphibole in CMASH here are noticeably different from those proposed by Oba (1978), who for experiments on a bulk composition corresponding to ts: $Ca_2(Mg_3Al_2)(Si_6Al_2)O_{22}(OH)_2$, proposed the breakdown reaction as the dehydration

$$\text{Amp} = \text{Pyp} + \text{Cpx} + \text{Opx} + \text{Qtz} + H_2O \qquad (28)$$

where quartz is a product rather than a reactant for this amphibole and a garnet composition close to $(CaMg_2)Al_2Si_3O_{12}$.

Although the work of Oba (1978) extends the breakdown reactions of amphibole to 24 kb, we cannot relate the reported assemblages to the starting composition in most of his experiments (see our fig. 2B).

Reaction (27) occurs below 875°C at 23 kb (table 3 and fig. 8). Reactions (26) and (27) have been investigated experimentally (here and

Ellis and Thompson, 1986) and must lie at higher temperatures than the quartz absent but water excess reactions

$$\text{Amp} + \text{V} = \text{Anr} + \text{Cpx} + \text{Opx} + \text{L} \tag{29}$$

and

$$\text{Amp} + \text{V} = \text{Pyp} + \text{Cpx} + \text{Opx} + \text{L} \tag{10}$$

Reactions (26) and (27) are shown in figure 8 to limit the stability of amphibole in CMASH in the absence of excess fluid. Also shown are schematic lines for the mole fraction of H_2O dissolved in the melt at the solidus (for example X_w^m in fig. 16.6 of Burnham, 1979b, p. 460). These lines probably refract toward higher temperatures when garnet and pyroxene replace plagioclase, approximately paralleling the appropriate dry solidus. The low pressure dehydration-melting of amphibole (to Anr + Cpx + Opx + Qtz + L, reaction 26) cuts across only a small range in the X_w^m isopleths in figure 8, (see also the discussion by Burnham 1979a, p. 473, for hornblende in basaltic melts).

The distinct backbending of the higher pressure fluid-absent melting of Amp (to Pyp + Cpx + Opx + Qtz + L, reaction 27) strongly cuts across lines of increasing X_w^m (fig. 8). This indicates that the amount of melt decreases noticeably along the fluid absent solidus represented by (27) toward higher pressures and lower temperatures. Thus for a given H_2O-content of a system (modal amount of amphibole), maximum melt production occurs at the lowest values of X_w^m at the highest temperatures. This occurs, according to the schematics in figure 8, around 5 to 10 kb when anorthite is among the dehydration-melting products of amphibole and around 15 kb when garnet replaces anorthite. Because the solubility of H_2O in "basaltic" melts increases along the H_2O-saturated solidus to higher pressures (Burnham, 1979b), then for a fixed amount of amphibole in the starting composition, melt production will be minimal in the vicinity of intersection of the high pressure dehydration melting reaction (27) and the appropriate H_2O-saturated solidus (here around 27 kb, 800°-825°C; figs. 3 and 4).

An important point is that dehydration melting of amphibolite liberates only a finite amount of water into an undersaturated melt. Upon ascent this melt becomes even more H_2O-undersaturated (crossing the X_w^m lines in fig. 8) and thus even less likely to develop peraluminous character simply by restite unmixing. Water solubility curves (fig. 8) show roughly how much water is necessary to saturate a melt at lower pressures, and the only way to increase this amount (by factors of 3-4) is thus by crystal fractionation.

It was noted above that the amount of melt produced depends both upon the amount of H_2O available (amphibole) and the value of X_w^m at a particular P and T. Thus along the amphibole dehydration melting curve, (reaction 27) in figure 8 the amount of melt is lowest close to the intersection with the H_2O-saturated solidus near 25 kb, 800°C. The

amount of melt produced increases as this reaction moves toward lower pressures and higher temperatures. The maximum amount of melt production occurs along the lower pressure segment (reaction 26), where Anr is stable at the highest temperature compared to the lowest X_w^m. Only melts produced along the positive dP/dT lower-pressure dehydration-melting curve (reaction 26) could rise to the surface without recrossing into the Amp field (see Ellis and Thompson, 1986 for further discussion). All melts produced along the negative dP/dT higher-pressure dehydration-melting curve (reaction 27) would upon ascent pass back into the Amp stability field, recrystallizing amphibole and removing H_2O from the magma. Only by extremely rapid ascent up an open fracture could such melts erupt.

These observations provide a general model for the degree of melt production for a given amount of amphibole in a rock as a function of pressure and temperature. Moreover the values of X_w^m may be estimated graphically if the solid-phase compositions are known. The compositions of phases are projected in figure 6 from $CaMgSi_2O_6$ and SiO_2 onto $CaAl_2Si_2O_8$ + $MgSiO_3$ + H_2O, in molar units. The molar H_2O-content of the melts at water saturation are shown for experiment Z-24E (at 900°C/15 kb, table 4), recalculated first with the difference (100-oxide probe total wt percent), and second, by arbitrarily adjusting the H_2O content to 10 wt percent (using 260 as the gram formula weight for the melt). Figure 6 shows that the topology is governed by the possible projected colinearity (L-Amp(~tt)-Ens) in the presence of Cpx + Qtz.

OTHER DEHYDRATION-MELTING REACTIONS IN CMASH

Zoisite, talc, and amphibole are, in principle, all capable of undergoing dehydration melting to yield water-undersaturated melts (fig. 6). However the calculations using available thermodynamic data bases (app. 2) show that Zoi + Tal + Qtz is not stable near the H_2O-saturated solidus in CMASH. However, Tal + Amp + Qtz stability (talc-amphibolites) overlaps the H_2O-saturated solidus below about 6 kb (fig. 8), and Zoi + Amp + Qtz (epidote-amphibolites) overlaps the H_2O-saturated solidus from about 8 to near 20 to 25 kb (app. 2 and fig. 8). An additional dehydration-melting reaction to be considered is

$$\text{Zoi} + \text{Amp} + \text{Qtz} = \text{Anr} + \text{Cpx} + \text{L} \qquad (30)$$

Higher pressure dehydration-melting reactions are different for the two cases of reaction sequences as illustrated in figure 7. For case A (fig. 7) the reaction

$$\text{Zoi} + \text{Amp} + \text{Qtz} = \text{Cpx} + \text{Pyp} + \text{L} \qquad (31)$$

occurs between about 15 to 18 to 25 kb (compare fig. A-1 and C). For case B (fig. 7) the reaction in this pressure range would be

$$\text{Zoi} + \text{Amp} + \text{Qtz} = \text{Cpx} + \text{Kya} + \text{L} \qquad (32)$$

According to the schematics in figures 7 and 8, reactions (30) and (31) meet the fluid-absent melting reaction

$$\text{Anr} + \text{Amp} + \text{Qtz} = \text{Pyp} + \text{Cpx} + \text{L} \qquad (33)$$

which marks the upper-pressure stability limit of quartz-bearing amphibolites in CMASH. Reaction (33) has been located in figures 6 and 8 to join with reaction (1).

Reactions (27) and (31) are located in figure 8 and converge near 800°C and 26 kb. This P-T region is of particular importance, because it is the overlap of the dehydration melting reaction (27), the subsolidus dehydration of amphibole in CMASH (17), the upper stability of talc (4), and the H_2O-saturated solidus. The results for CMASH certainly indicate that epidote-amphibolites will undergo dehydration-melting at temperatures above the H_2O-saturated solidus (near 800° to perhaps 850°C from about 10 to 20 to 25 kb). These temperatures are significantly lower than the dehydration-melting of epidote-free natural amphibolites (above 900°C, Rushmer, 1991) at pressures corresponding to the continental Moho ($\sim$ 10 kb).

SOME APPLICATIONS OF THE CMASH EXPERIMENTS TO AMPHIBOLITE MELTING

In order to understand the dehydration-melting reactions that can occur along different P-T paths, composition diagrams for quartz- and clinopyroxene-bearing assemblages projected onto $CaAl_2Si_2O_8$–$MgSiO_3$–H_2O (using the format of fig. 6) have been included in figure 7. Amphibolite compositions, with only the water bound in hydrous minerals, plot near the base line of each triangle. These may be located in P-T space by reference to figure 8.

At pressure below about 7 kb only one fluid-absent melting reaction (26) is encountered around 900°C. At pressures between 7 and 25 kb a lower temperature dehydration melting reaction involving talc could occur around 800°C. Both these reactions could only occur in epidote-free amphibolites.

Epidote-bearing amphibolites undergo at least two dehydration-melting reactions between 10 and 20 to 25 kb. In the pressure range 10 to 15 kb, Zoi + Amp + Qtz melt to produce Anr + Cpx + L, and in the range 15 to 20 to 25 kb these produce Gar + Cpx + L (case A) or Kya + Cpx + L (case B)—as illustrated for H_2O-undersaturated melts in figures 7 and 8. For case B, Amp + Kya assemblages (fig. 7) could undergo a second dehydration-melting episode before the third Amp-out dehydration melting (27). The strongly negative dP/dT of these reactions above 15 kb and that for Amp-out (27) causes the dehydration melting to move to lower temperatures with increasing pressure into the overlap region near 26 kb, 800°C.

The results of the experiments in CMASH are shown by solid lines in figure 9 compared to those for natural basaltic compositions (dashed lines). The amphibole stability here is compared to the fluid-absent melting results of Rushmer (1991) on basaltic amphibolite. It can be seen

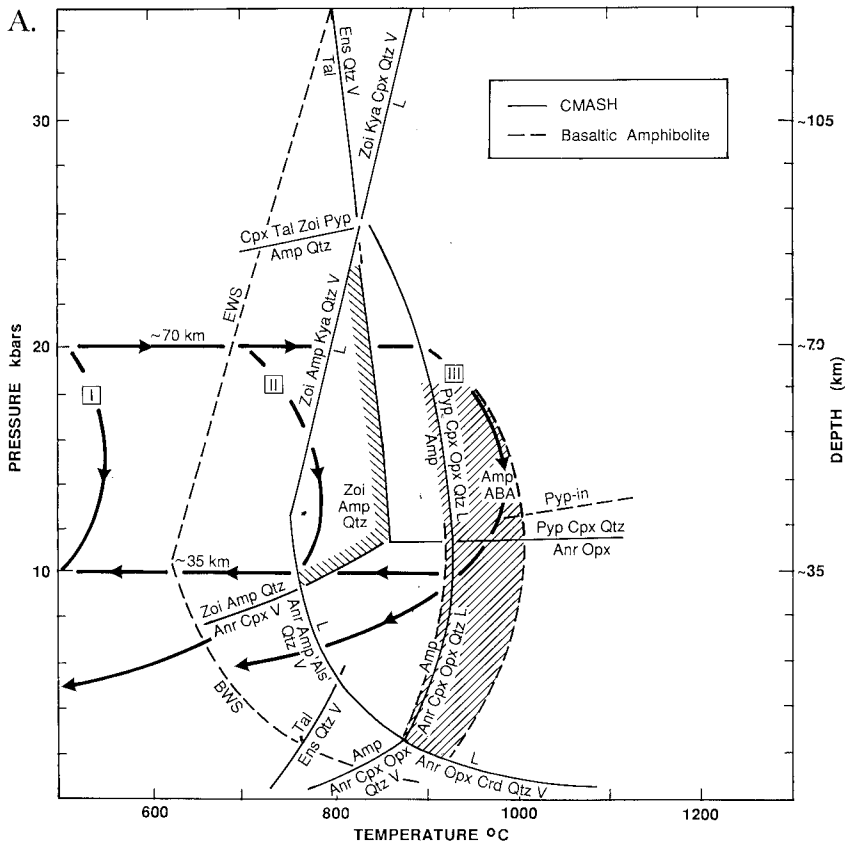

Fig. 9. Pressure-temperature diagram showing the H_2O-saturated solidus and the fluid absent melting of amphibole in CMASH compared to the H_2O-saturated solidii for basalt—BWS and eclogite—EWS (Helz, 1976; Yoder and Tilley, 1962; Lambert and Wyllie, 1972) and the fluid absent-melting of basaltic amphibolite (at 8 and 18 kb; Rushmer 1991). The fluid-absent melting of amphibole in CMASH coincides with the beginning of amphibole melting in basaltic amphibolite indicating that the effect of Na in stabilising amphibole to higher temperatures has a greater effect than Fe in lowering the amphibolite fluid-absent solidus. The diagonally hatched areas represent the fluid-absent melting interval in amphibolite (Rushmer, 1991).

Most PTt paths for continental collision (England and Thompson, 1986) do not result in fluid-absent melting of amphibolite (in A). Only very-hot subduction zone paths (Peacock, 1991) can result in dehydration-melting of amphibolite (in 9B). Subduction zone path C in (9B) passes through the P-T region where Zoi + Amp disappear from basaltic compositions, roughly coincident with talc disappearance from hydrated mantle. This fertile region for melt production, although obtained here for CMASH, most probably applies also to natural amphibolite compositions.

that our results in CMASH coincide with the lower bound for basaltic amphibolite dehydration-melting (the melting interval is shown by the shaded region in fig. 9). Because amphibolites contain Na and Fe in excess of CMASH, the near identical location of the beginning of amphibolite dehydration-melting with the solidus in CMASH means that the

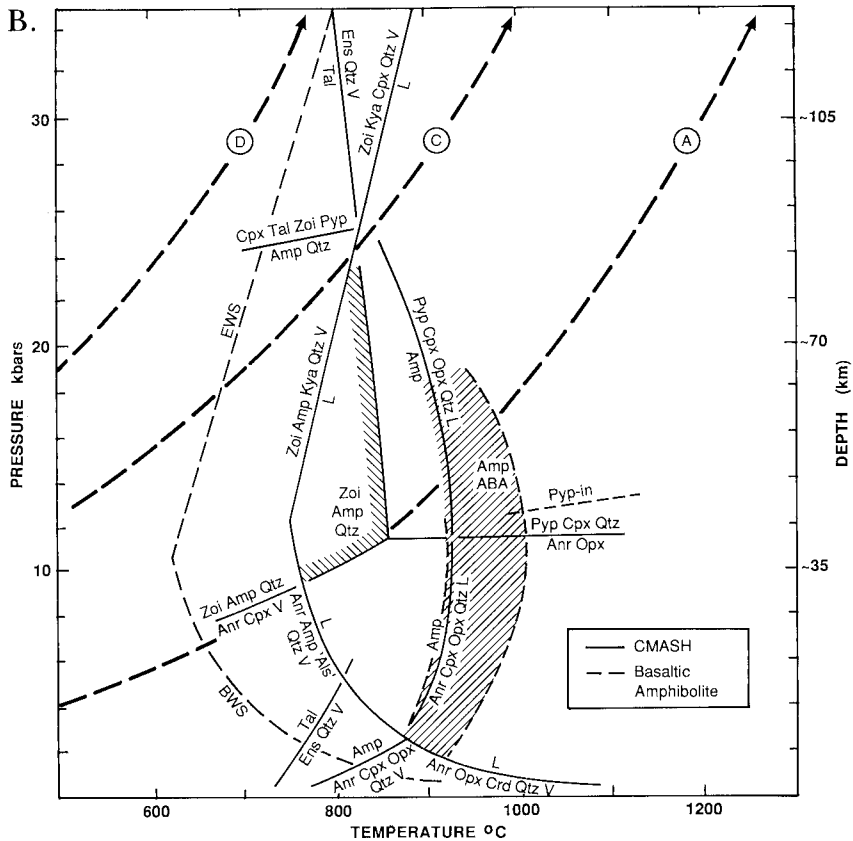

Fig. 9B

up-temperature displacement due to Na is much stronger than the down-temperature displacement due to Fe.

The H_2O-saturated solidus in CMASH (fig. 9) lies some 100° to 125°C higher than the H_2O-saturated solidus for basalt (BWS, from Helz, 1976) and for eclogite (EWS, from Lambert and Wyllie 1972).

As noted with regard to figure 8, the dehydration of Zoi + Amp strongly overlaps the H_2O-saturated solidus in CMASH (in fig. 9). According to the calculations of Evans (1990) for basaltic compositions, epidote-bearing blueschists do not cut the H_2O-saturated solidus for basalt. However, natural epidote-amphibolite assemblages appear to be stable to temperatures higher than the wet solidus for basalt, according to the petrogenetic grids of Abbott (1982) and the experiments of Poli (1993), Schmidt (1993), and Schmidt and Thompson (1993).

PTt paths for thermal relaxation of collision thickened continental orogenic belts for "reasonable" initial geotherms and radioactive heat-distribution (England and Thompson, 1984, 1986) are shown by heavy

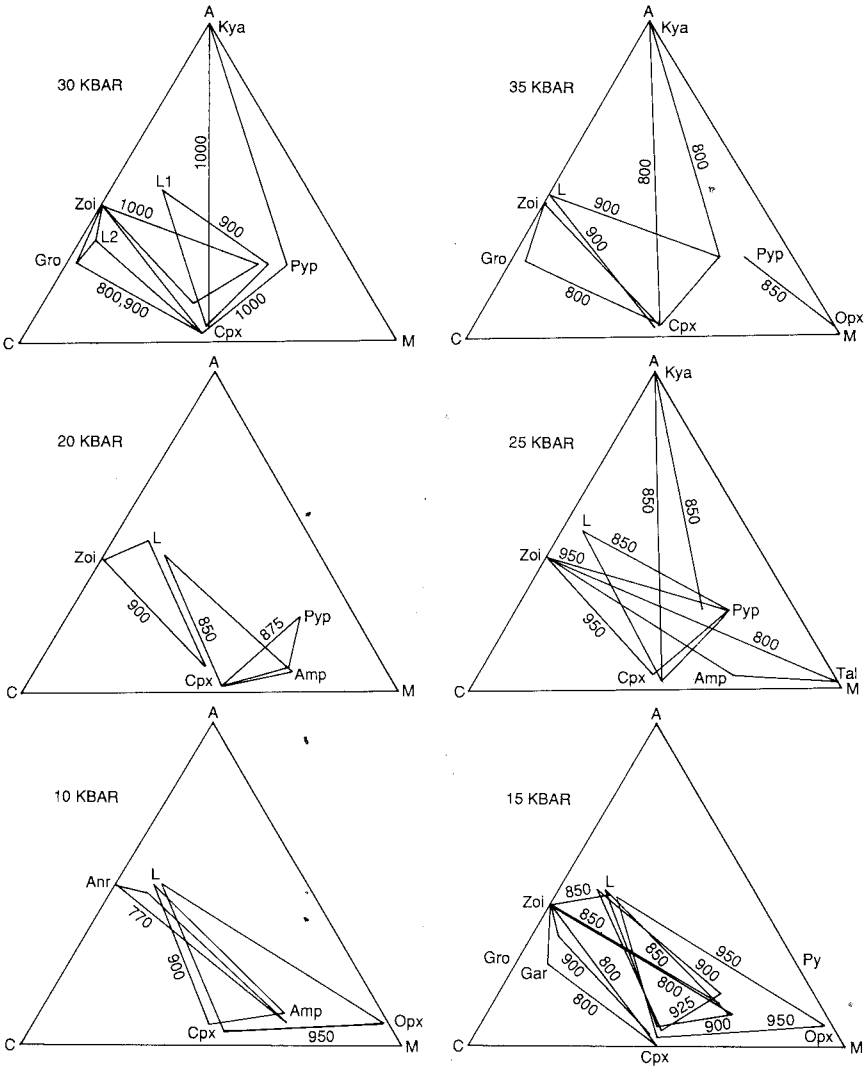

Fig. 10. Isobaric polythermal ACM diagrams showing the compositions of minerals and melts from H_2O excess (saturated) experiments at 10, 15, 20, 25, 30 and 35 kb. Quartz and water-saturated assemblages as opposed to those in which quartz has been removed by the formation of water-saturated siliceous melts can be determined from table 3. All melts from mafic compositions are peraluminous. From 15 to 35 kb at low temperatures the percalcic part of the system undergoes eutectic melting (Gro + Cpx + Zoi + Qtz + V = L_2). This relationship is not shown at all pressures for simplicity.

lines marked I and II in figure 9A. These PTt paths do not cross the dehydration-melting curve for basaltic amphibolite (Rushmer, 1991). This restricts the source of I-type granites to earlier dehydration-melting reactions involving orthoamphibole or biotite (island-arc tholeiite of

Rushmer, 1991) or requires very hot initial geotherms (path III in fig. 9A) preceding relaxation of collision thickened continental crust (England and Thompson, 1984, Heat Source Distribution III) or more likely an additional heat source. This heat source could be raised asthenosphere following tectonic extension of overthickened continental crust (Wickham and Oxburgh, 1988; Thompson, 1990), basalt input into a thickened crust, or delamination of a dense eclogite root (Thompson, 1990; Ellis, 1992, and references therein). However, some PTt paths (between II and III in fig. 9A.) would cross the dehydration-melting of epidote-amphibolites in CMASH between about 10 and 20 to 25 kb.

Shown in figure 9B are some steady-state paths appropriate to the subduction of oceanic crust with various thermal histories (Peacock, 1991, fig. 3, geotherms A and D; our geotherm C is somewhat hotter than that illustrated by Peacock). As discussed by Peacock, Rushmer, and Thompson (1994) only very hot subduction geotherms cut amphibole dehydration-melting reactions in natural compositions (path A in fig. 9B). Paths for subduction of cold mature lithosphere (D and C in fig. 9B) will show subsolidus dehydration of amphibole assemblages but not melting of hydrated oceanic crust. Thus normally the slab will not melt, unless water is coming in from elsewhere (see also Peacock, 1991).

Clearly the amount of melt produced by dehydration-melting depends upon the quantity of amphibole and zoisite in the basaltic protolith (and serpentine in the underlying peridotite) compared to the amount of H_2O that can be dissolved in calc-alkaline melts at any particular pressure and temperature.

SOME APPLICATIONS OF THE CMASH EXPERIMENTS TO MAGMA GENERATION AND FRACTIONATION

As stated near the beginning of this paper the present experimental results on CMASH, when combined with our earlier study (Ellis and Thompson, 1986) and those of other workers on natural mafic compositions, enable us to consider several distinct P-T regions for magma generation and fractionation. It is important first to emphasize the major differences in melt composition produced by H_2O-saturated compared to fluid-absent (dehydration) melting. Melt compositions from these high pressure experiments on CMASH (fig. 10) and natural basalt/amphibolite are in similar locations to those up to 15 kb pressure plotted in figure 10 of Ellis and Thompson (1986).

The compositions of melts from H_2O-saturated experiments in CMASH and on amphibolites.—The present experiments have shown that water- and quartz-excess melting of model basaltic compositions in CMASH produced siliceous and peraluminous liquids at temperatures close to the solidus from 5 to 35 kb (figs. 10 here and Ellis and Thompson, 1986, fig. 10).

All the melts up to 950°C at all pressures (fig. 8) are peraluminous and plot below the $CaAl_2SiO_6 + Mg_2SiO_4 + SiO_2$ plane in figure 2A. Although some of the melts shown in figures 2A and 8 are projected from

SiO_2, the absence of quartz in these run products does not change their peraluminous nature.

The lowest temperature melts were produced in peraluminous systems (that is Anr + Opx; Anr + Tal; Zo*i* + Tal; Zo*i* + Opx with Crd or Kya); thus the thermal divides are broken close to the quartz- and water-saturated solidus permitting Amp, then Cpx, to coexist with peraluminous melts.

In the lower pressure region (below 10 kb), where Anr + Opx (or Talc) are involved in the melting, the melts are clearly peraluminous (in the conventional sense), up to at least 950°C under H_2O-excess conditions (Ellis and Thompson, 1986). As illustrated by the ACM projected compositional triangles (from SiO_2 and H_2O) in figure 10, the melts from model basaltic compositions remain peraluminous until at least they coexist with Cpx + Amp or with Cpx + Opx. Certainly at 1 atm dry, the melts are eutectic to Anr + Opx + Cpx + (Qtz) (see Ellis and Thompson, 1986) and are therefore diopside normative. Helz (1976) in her study of basalt melting at 5 kb P_{H_2O} also produced peraluminous melts for the first 300° of melting and at about 1025°C the melts changed from corundum to diopside normative.

In their water-saturated melting study of a model quartz-eclogite in CMASH at 30 kb, Sekine, Wyllie, and Baker (1981, p. 947, their fig. 4b) also show their melts from 900° to almost 1100°C are peraluminous (Cor-normative) and with even higher percentages of melting above 1100°C are metaluminous (Dio-normative). However as emphasized above, because water-saturated melting at pressure greater than about 12 kb (fig. 6) involves ziosite and not anorthite, the conventional definition of peraluminosity loses meaning.

In the H_2O-saturated experiments on natural basaltic compositions of Beard and Lofgren (1991), the melts formed at 3 and 6.9 kb were strongly peraluminous, rich in Ca, and poor in Fe, Mg, Ti, and K. Beard and Lofgren (1991) considered these H_2O-saturated melts to be unlike those of most natural silicic melts (see also Carroll and Wyllie, 1989). Cawthorn and Brown (1976) and Cawthorn and O'Hara (1976) showed that amphibole fractionation from calcalkaline/basaltic compositions led to peraluminous later melts.

An important point from the lower pressure experimental study of Ellis and Thompson (1986) (region 1 in fig. 4) was the observation that Dio-normative, intermediate source rocks under H_2O-excess conditions produce minimum melts which are peraluminous (Cor-normative). The fact that this occurs in the CMASH system can thus be confidently ascribed to the breaking of the norite thermal divide (Anr + Opx) rather than to additional components. The transition from earlier metaluminous to later peraluminous compositions is a well known compositional feature of the most felsic members ("minimum melts") of most I-type granite suites (White and Chappell, 1977). This observation was noted earlier from natural rock experiments (see Ellis and Thompson, 1986 for

references) and has been confirmed by a number of observations on natural rocks (Helz, 1976; Conrad, Nicholls, and Wall, 1988).

The compositions of melts from dehydration melting experiments in CMASH and on amphibolites.—While H_2O-saturated melting in CMASH produces Cor-normative melts, fluid-absent (dehydration-) melting produces Dio-normative melts from a Dio-normative initial composition in the presence of plagioclase (see Ellis and Thompson, 1986). This has been confirmed for natural rock experiments at pressures within the stability field of plagioclase (see Conrad, Nicholls, and Wall, 1988; Rushmer, 1991; Beard and Lofgren, 1991).

Rushmer (1991) found that dehydration melts from basaltic amphibolite were tonalitic and meta-aluminous at 8 kb (involving Amp + Plg + Qtz). Beard and Lofgren (1991) experimentally studied five metamorphosed basalts and andesites and found that under dehydration-melting conditions (defined as no additional water than that bound in hydrous minerals) the melts were of only mildly peraluminous to metaluminous compositions. Their analyzed melts corresponded to granodioritic and tonalitic-trondhjemitic intrusives and similar to silicic rocks in modern oceanic arcs but apparently not as peraluminous as many felsic I-type bodies. Thus, dehydration (fluid-absent) melting of mafic (Dio-normative source rocks) within crust of normal thickness ($\sim$35 km) where plagioclase is stable produced only weakly peraluminous to metaluminous (Dio-normative) minimum melt compositions.

However, the present study has shown that at higher pressures than the stability limit of plagioclase, minimum melts from a mafic-intermediate source are peraluminous, irrespective of whether they are fluid-saturated or dehydration-melting products. Higher pressure melts are characterized in nature (Arth and Hansen, 1972; Arth and others, 1978; T. H. Green, 1982, 1992; Rapp, Watson, and Miller, 1991) by distinct geochemical signatures indicative of both residual garnet and an absence of plagioclase (for example, HREE and Y depletions, high La/Yb ratios, high Sr, and general absence of an Eu anomaly). Such melts therefore must form in the lower parts of thickened crust, or thickened arcs, or subducted slabs, and differ from the more common I-type granites. For example, those from the Lachlan Fold Belt of eastern Australia appear to have been formed by intracrustal melting of a normal thickness crust (Ellis, 1987).

Water and I-type granitoids and intermediate rocks.—Current models generally propose that I-type granite suites form by fluid-absent dehydration-melting of a hornblende-bearing mafic to intermediate composition source (Chappell and Stephens, 1988), and specific arguments for the general importance of fluid-absent melting have recently been reviewed by Clemens (1990). However the "minimum" melts in many of these suites are in fact strongly peraluminous. We note that although this and other experimental studies have shown that peraluminous "minimum" melts may be satisfactorily modelled by partial melting of a metaluminous

source, we have found that this can best be achieved in the presence of an excess free fluid phase.

Thus the general view of the prevalence of dehydration-melting within the crust may be considered to be at variance with the experimental requirement of excess fluid conditions for such I-type suites at the beginning of melting. To these points then we offer the following suggestions.

The restite model of White and Chappell (1977) proposes the geochemical variation within an I-type granite suite to be controlled by the degree of physical separation of a restite material from the minimum melt composition formed at source. This minimum melt is peraluminous, and with increasing amounts of mafic restite a rock suite trends toward metaluminous, Dio-normative compositions (see Ellis and Thompson, 1986, for fuller discussion). Our preferred explanation is that these I-type suites did indeed form by higher temperature dehydration melting as proposed by White and Chappell (1977) and Clemens (1990), but that the magmas produced would have metaluminous minimum melts (see Ellis and Thompson, 1986). We would then suggest, based on the above experimental observations, that the I-type rocks analyzed by White and Chappell (1977) with peraluminous "minimum" melt compositions are not those that formed upon fluid-absent partial melting. They probably represent the later, lower temperature melts which formed by conventional crystal-liquid equilibria processes as successively lower temperature melts evolved toward fluid saturation and thus toward Cor-normative compositions. Several I type suites trending to Cor-normative minimum melts do show evidence in trace element abundances for extensive crystal fractionation in the more felsic types (Mahood and Halliday, 1988; Halliday and others, 1991; Champion and Chappell, 1992).

SOME ADDITIONAL GEOLOGICAL APPLICATIONS

The material presented here provides a background model over a large range of P-T space (to 40 kb, 600°-1000°C) appropriate to subsolidus dehydration and dehydration-melting of common hydrous minerals in subduction zones, continental collision belts, and continental extensional terrains.

Minimum melts in the CMASH system at deep levels (> 10 kb) involve zoisite; epidote does occur in some plutonics and volcanics (Hollister, 1982; Zen, 1985; Hammarstrom and Zen, 1986). Such magmas, if they are formed below 800°C, can be partial melting products of lower continental crust tectonically thickened by continental collision without needing additional heat input, or of subducted oceanic crust. In contrast, melting of zoisite-free amphibolites appears to require an additional heat source to reach the higher temperatures necessary for fluid absent melting. This may be the reason why mafic migmatites are so rare.

Some I-type granite terrains appear to be generated by basalt addition to non-thickened crust (for example, the Lachlan fold belt,

Australia, which has ~400 Ma granites and coeval volcanics still preserved). If there had been tectonic thickening and uplift/erosion as in the cases above, then there would be no chance that volcanics erupted on a land surface would still be preserved—and still within a few kilometers of sealevel (Ellis, 1987).

One problem that can be addressed by the present study is to what extent dehydration occurs in subducted oceanic crust, or whether the H_2O remains bound in hydrous minerals deeper than the depth of generation of arc magmas (100–125 km, Gill, 1981). The region near 25 to 30 kb near 800°C in CMASH involves the near simultaneous dehydrations of Zoi + Amp, Amp + Kya, and Amp-alone (figs. 9B and A-1C) very close to the H_2O-saturated solidus. Furthermore the dehydration reaction of talc also passes through this region. Serpentine, the likely hydrous phase in the hydrated mantle part of the lithosphere, appears to dehydrate below 700°C in the 25 to 35 kb range. Thus a subduction geotherm close to path B in figure 9B would encounter simultaneous dehydration in epidote- and amphibole-bearing subducted oceanic crust as well as serpentine and talc in the underlying mantle. This would result in a greater amount of melt being produced in the overlying mantle wedge through dehydration fluid interacting with hot mantle than simply through dehydration-melting of subducted basalt (Kesson and Ringwood, 1989).

The present experiments and future ones on the dehydration-melting of the three subducted slab components (sediment, oceanic crust, partially hydrated mantle) will help to evaluate the H_2O-subduction budget (Peacock, 1990; Thompson, 1992). Careful mass balance between dehydration and magma generation beneath convergent arcs, in the depth range 50 to 120 km, is required to quantify fully the quantities of water likely to be subducted past the depth of generation of arc magmas.

ACKNOWLEDGMENTS

The project was started while D. J. Ellis was supported at ETH Zürich by the Schweizerische Nationalfonds and was completed at the Australian National University (with assistance of ARC funding). Rolf Schmid gave technical support with the Zürich piston-cylinder apparatus. We thank James Connolly for generous help in using his program VERTEX. We are pleased to acknowledge discussion with Tim Holland, Stefano Poli, Tracy Rushmer, Max Schmidt, Peter Ulmer, Peter Wyllie, and review by James Beard.

We thank Mary Hope (ANU), Ursula Stidwill, and Brigitt Marques (ETH) for typing and Kevin Cowan (ANU) for drafting.

APPENDIX 1

Experiments were carried out on a series of glasses, glasses plus synthetic minerals, and mineral mixes with varying compositions in the $CaO–MgO–Al_2O_3–SiO_2–H_2O$ system. All starting compositions were quartz excess in the subsolidus region (table 3). The locations of these compositions on an ACM diagram with respect to minerals of interest are shown in

figure 2A. Unlike previous studies in this system in which a specific bulk composition was used, our aim was to document the P-T stability fields of specific mineral assemblages. The $CaMg_{-1}$ and $Al_2Mg_{-1}Si_{-1}$ substitutions in some phases necessitated the use of a large number of starting compositions as any one composition was not adequate for crystallizing critical mineral assemblages over a broad P-T interval.

Synthetic glasses were prepared by thoroughly mixing AR grade oxides (Al_2O_3, SiO_2) and carbonates ($CaCO_3$, $MgCO_3$) together and then melting them to quench crystal-free glasses using an iridium strip heater (see Nicholls 1974). Molten glasses were stirred with a Pt rod to enhance homogeneity and then quenched in a jet of air. These glasses were then ground to >10 μm size in an agate mortar further to enhance chemical homogeneity of each 10 mg aliquot used for each experiment. Three or four large glass fragments were analyzed with an electron microprobe to check the starting compositions (table A-1).

Anorthite, zoisite, enstatite, pyrope$_{70}$-grossular$_{30}$, diopside, and tremolite were synthesized from AR grade oxides (table 4). Orthorhombic zoisite was the stable polymorph found in our experiments, consistent with the experimental studies by Jenkins, Holland, and Clare (1983) on the relative stabilities of zoisite and clinozoisite.

Tremolite of composition $Ca_2Mg_5Si_8O_{22}(OH)_2$ could not be synthesized but is always subcalcic ($Ca_{1.9}Mg_{5.1}Si_8O_{22}(OH)_2$) as evidenced by the presence of diopside as a synthesis run product, confirmed by microprobe. This problem has been noted previously (Boyd, 1959; Troll and Gilbert, 1972; Wones and Dodge, 1977). Chatterjee (personal communication, 1971 to Wones and Dodge, 1977) made a rigorous study of this problem and concluded that tremolite synthesized at 750°C contains 5 to 10 molecular percent $Mg_7Si_8O_{22}(OH)_2$—see also Welch and Pawley (1991) and Jenkins, Holland, and Clare (1991).

High pressure experiments were carried out using piston cylinder apparatuses at Zurich and the University of Tasmania. Pressure assemblies were similar in both laboratories. Experiments using talc as a pressure medium had a −10 percent friction correction applied (see D. H. Green and Ringwood, 1967b, p. 771), whereas those using NaCl had no friction correction (see Johannes and others, 1971). A piston-in technique was used. Experimental techniques are similar to those described by Green and Ringwood (1967b). Temperature was measured using $Pt/Pt_{90}Rh_{10}$ thermocouples, and temperature was controlled automatically to within ± 5°C.

Each experiment had 10 mg of starting material together with up to 3 mg of water sealed inside Pt, $Ag_{75}Pd_{25}$ or $Ag_{50}Pd_{50}$ capsules. Capsule weights were noted before and after each experiment in order to determine if H_2O had escaped. Excess water was determined on the basis of a fluid phase bubbling out of the capsule upon piercing. Water excess experiments that did not meet these criteria were not used in the interpretations. Primary vapor was identified in polished mounts by large vesicles in glass, orders of magnitude larger than the micron sized quench vapor exsolved from glass on quench.

Run products were examined optically using immersion oil grain mounts, X-ray diffraction and polished fragments analyzed using the energy dispersive SEM-microprobe at the University of Tasmania. Full ZAF correction procedures were employed (Griffin, 1979). Where feasible, both cores and rims of minerals were analyzed to check for zoning. In these cases where interference from other phases was encountered during analysis, the more stoichiometric analyses were taken as the equilibrium composition. Where zoning or inhomogeneity existed, compositional ranges are reported in the tables of run product compositions.

Melt (liquid) in this system quenched to a clear glass devoid of quench crystals or overgrowths to primary crystals (in contrast to Na_2O-bearing systems). Run products below the solidus were generally friable and easily ground in an agate mortar. The presence of melt corresponded with a much denser sample and a greater difficulty in grinding fragments for optical examination.

TABLE A-1

Starting mix compositions

Except for Al and Bl about 20 wt percent water was added to all mixes

A 1 = Glass A + 10 wt percent zoisite
B 1 = Glass B + " " " "
A 2 = Glass A + 20 wt percent mix 1
B2 = Glass B + " " " "
E 2 = Glass E + " " " "
A 3 = A 2 + 10 wt percent quartz
B 3 = B 2 + " " " "
E 3 = E 2 + 20 " " "
A 4 = 90 percent (.43 Glass A + .57 Z-8) + 10 wt percent quartz
E 4 = 80 " (3 $Mg_2Si_2O_6$ + 4 $CaAl_2Si_2O_8$ + 2$CaMgsi_2O_6$) + 20 wt percent quartz

Mineral Mix 1 = 4 Diopside + 1 Anorthite + 1 Zoisite

	Glass A	Glass B	Glass E	A 1	B 1	A 2	B 2	E 2	A 3	B 3	E 3
SiO_2	46.44	49.61	44.65	45.76	48.62	46.88	49.41	45.44	52.19	54.47	56.35
Al_2O_3	20.18	18.57	23.85	21.53	20.08	19.32	16.86	21.09	17.39	15.17	16.87
MgO	9.97	6.02	14.48	8.97	5.42	9.98	4.82	11.58	8.98	4.34	9.26
CaO	23.41	25.82	17.04	23.53	25.71	23.61	25.54	18.52	21.25	22.99	14.82
H_2O				0.20	0.20						
A	22.9	23.01	26.08	24.7	24.9	22.1	22.3	25.1	22.1	22.3	25.1
C	48.4	58.14	33.89	49.2	58.0	49.1	61.5	40.1	49.1	61.5	40.1
F	28.7	18.7	40.03	26.1	17.0	28.8	16.2	34.8	28.8	16.2	34.8

	A 4	E 4	Mix 1	Run Z-8
SiO_2	59.0	60.27	48.62	60.50
Al_2O_3	7.81	15.18	15.86	0.0
MgO	16.87	12.01	10.03	25.38
CaO	16.30	12.53	24.43	14.12
H_2O			0.56	
A	9.7	22.2	18.5	0.0
C	37.0	33.3	51.9	28.6
F	52.3	44.4	29.6	71.4

Glasses were easily recognized with the SEM microprobe. Both point analyses and area scans of glasses were made to check for homogeneity. Glass analyses totalled up to 84 wt percent oxides. The difference from 100 percent does not correspond to the actual water content, in contrast to other proposals (Beard and Lofgren, 1991, p. 369) for lower pressure experiments. Microprobe analyses of glasses with known water contents result in probe

totals where differences from 100 wt percent are in excess of the actual water content (see Ellis and Thompson, 1986).

Appendix 2

Calculation of melt-absent equilibria in CMASH using thermodynamic data bases

During the period June 1990 to December 1992, considerable effort was devoted to using thermodynamic data bases to compute melt-free equilibria. The chronology here is important to state because during this time, thermodynamic parameters for several endmember minerals in CMASH have been changed in the data bases. This can be seen for example by comparing reaction (1) among Tal, Ens, Qtz, H_2O in figures A-1A and B with B. In this case minor changes to the petrogenetic grids are introduced for mafic compositions in CMASH.

The strategy used in the calculations was to use a current mineral endmember thermodynamic data set with various models for crystalline solution in amphibole, garnet, and pyroxene. The results of the calculations of petrogenetic grids for CMASH to 40kb and from 500° to 1100°C (fig. A-1A,B, and C) are therefore independent of the experimental data presented here. While involving enormous extrapolation over P-T space, the calculations in their various forms have tremendous bearing on the interpretation of the experimental results and vice versa.

Our intention here is not to concentrate upon individual merits or shortcomings of thermodynamic data bases. Rather we wish to illustrate where (in P-T-X space) there is major disagreement with experiments and to suggest what additional kinds of information is required to obtain better agreement.

It is important here to note that the upper stability limit of amphibole by dehydration, though metastable, encompasses the melting reactions leading to amphibole disappearance in P-T space (fig. 4). This result is implicit in the theoretical treatments of stable and metastable reactions around invariant points involving melting reactions with and without fluids (Ellis and Thompson, 1986, fig. 4). What is particularly useful here is that the metastable extensions of CMASH dehydration reactions (involving $Al_2Mg_{-1}Si_{-1}$ in [Amp] [Cpx] and $CaMg_{-1}$[Gar] reemerge in the subsolidus region as upper pressure limits to amphibole stability.

The thermodynamic data base of Holland and Powell (1990) uses the tt composition as the aluminous amphibole endmember $(Ca_2Mg_3(MgAl)Si_4(Si_3Al)O_{22}(OH)_2)$ with thermodynamic properties constrained by the experimental results of Jenkins (1988).

Both Léger and Ferry (1991) and Liebermann and Kamber (1991) have obtained thermodynamic parameters for the ts composition $(Ca_2Mg_2(MgAl_2)Si_3(Si_3\ Al_2)O_{22}(OH)_2$ from the experimental data of Jenkins (1987, 1988; see also Mäder and Berman, 1992) relative to the Berman (1988) data base for the buffering reaction

$$Al_2Mg_{-1}Si_{-1}[\text{Amp, Cpx}] = CaAl_2Si_2O_8 - CaMgSi_2O_6 - SiO_2.$$

The thermodynamic properties for the aluminous amphiboles used in the calculations are:

Amphibole	$\Delta G^\circ_{f(298,1)}$ J mol^{-1}	S°_{298} J mol^{-1}k^{-1}	$\Delta H^\circ_{f(298,1)}$ J mole^{-1}	Reference
ts	−11,800,684	538.6	−12,534,670	Léger and Ferry (1991)
ts	−11,716,444	542.72	−12,449,094	Liebermann and Kamber (1991)
tt	−11,691,390	551.0	−12,420,290	Holland and Powell (1990)

Attempts were made as part of this study to obtain additional thermodynamic data on CMASH amphiboles using the recent experimental results reported by Cho and Ernst (1991) for the equilibria

$$Ca_2Mg_5Si_8O_{22}(OH)_2[Amp] + 12Al_2Mg_{-1}Si_{-1}[Amp] = 2Ca_2Al_3Si_3O_{12}(OH) + 7Al_2O_3 + H_2O.$$

These results are of particular interest because according to their experimental results the $Al_2Mg_{-1}Si_{-1}$[Amp] vector increases with increasing temperature and decreasing pressure. This indicates that the assemblage with free H_2O (zoisite, corundum, tremolitic amphibole) is the low entropy assemblage. However, no satisfactory fits using this data could be obtained by us, nor by Dr. M. Cho (personal communication, 1991), nor by Dr. T. Holland (personal communication, 1992).

Several sets of calculations (three of which are shown in fig. A-1.) were performed using the program VERTEX (Connolly, 1990) with the two data bases and the amphibole data quoted above. The results of calculations using the Holland and Powell (1990) data set with one ideal mixing site are shown in figure A-1A, and the Berman (1988) data set with the Léger and Ferry (1991) amphibole data and assuming ideal mixing on four sites are shown in figure A-1B. Calculations were performed with an update of the Holland and Powell data set and using a multisite ideal model for amphibole and nonideal garnet (Berman, 1990) but ideal clinopyroxene solid solutions—the results are shown in figure A-1C.

The positions of equilibria in MASH, MSH, CMSH, and CASH using the two data bases and the different solution models are nominally identical. The principal differences lie in the location of Al-Amp reactions.

It is most useful to focus on these in terms of reaction-families, involving Al-amphibole, rather than seek out discrepancies among a myriad of reactions. The hydrated mineral reaction-families that are of prime concern here are the various reactions that involve Tal + Zoi, Amp + Zoi, Amp + Kya, and ultimate Al-amphibole stabilities. Their relative stabilities are emphasized by different kinds of shading in figure A-1A, B, and C.

It is appropriate to consider first the difference in reactions for the ultimate disappearance of Al-amphibole. All three sets (figs. A1A, B and C) show the metastable dehydration of Al-amphibole by the same reactions at temperatures higher than the experimentally located dehydration melting of Al-amphibole in CMASH (fig. 8)—consistent with the theories advanced above concerning figure 4.

The major differences result at higher pressures (25–35 kb) where the metastable Al-amphibole dehydrations intersect the talc-out reaction (1). It will be noted that discrepancies of almost 10 kb result for amphibole dehydrations with Tal and anhydrous minerals (fig. A-1A and B, see also fig. 1) and whether these reactions involve zoisite. The experimental results (table 3, runs Z-21', Z-27, T-14) would support more the reaction locations in figures A-1 and C but not B.

The location of the first reaction-family involving the ultimate stability of Al-amphibole (Amp-out) influences greatly the stability of the second reaction-family involving Tal + Zoi. The higher pressure stability of Al-amphibole in figure A-1b results in the Tal + Zoi stability being confined to temperatures below 550°C. This assemblage is stable to at least 700°C in figure A-1a and C, and to 800°C at 25 kb in our experiments (runs Z-27, Z-18). It should be emphasized that in all cases the reaction-family Tal + Zoi does not intersect the H_2O-saturated solidus in CMASH (fig. 3) for any of the calculated grids.

The remaining general problem concerns the two reaction-families with Amp + Zoi and Amp + Kya and how they interact with the others (Tal + Zoi and Amp-out). Considerable differences also exist here between the various calculations.

Figure A-1A shows that the Amp + Kya reaction in the region ~ 10 to 20 to 25 kb lies some 50° below but parallel to the Zoi + Amp reaction. This in turn influences the Zoi + Tal reaction-family at the intersection with Amp-out.

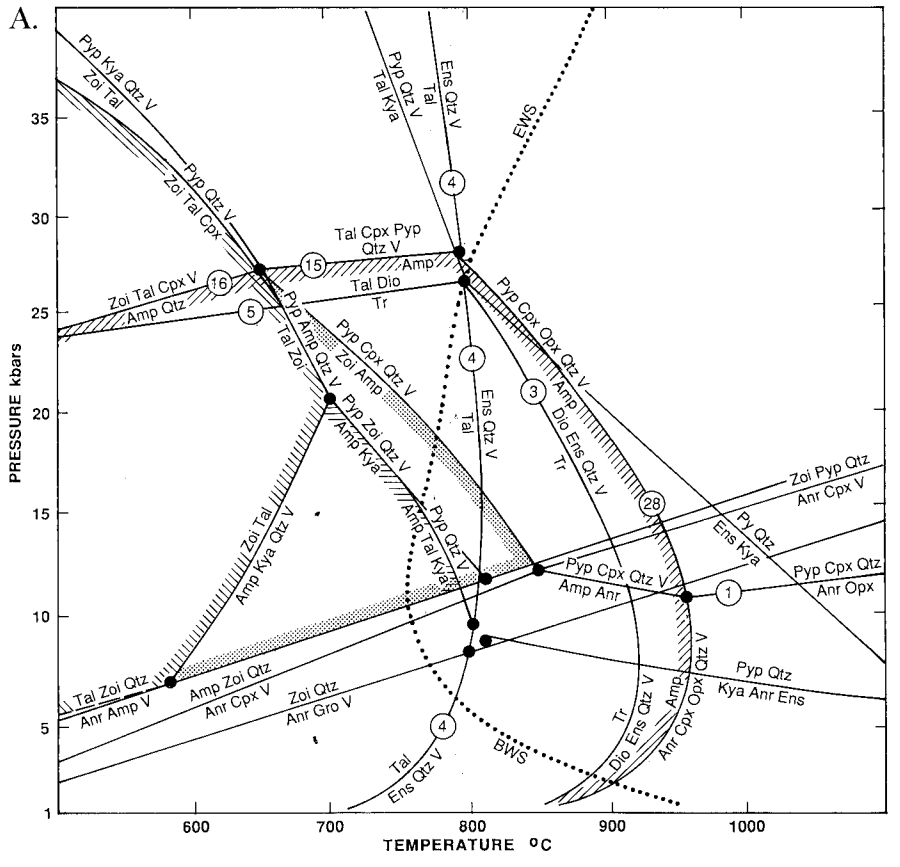

Fig. A-1A. Results of calculations of dehydration and solid-solid reactions in CMASH using the data bases of Holland and Powell (1990) and Berman (1988) with various solution models. The reaction families representing the stabilities of Tal + Zoi, Zoi + Amp, Amp + Kya and Amp-out (each with Qtz and H_2O) are shown by various shadings.

Figure A-1B shows that the Amp + Kya reaction intersects the Zoi + Amp reaction near 18 kb, 770°C. This intersection does not primarily influence the Zoi + Tal reaction-family but strongly interacts with Amp-out.

Figure A-1C shows that the Amp + Kya reaction-family lies at higher temperatures than Zoi + Amp. This strongly changes the sequence of reactions likely along the H_2O-saturated solidus in the region 15 to 30 kb.

It has been difficult not to incorporate the results of the thermodynamic calculations of reaction equilibria into the interpretation of our experimental data. Because we have concentrated our experimental efforts to developing an understanding of CMASH over a large range of P-T space (to 35 kb, 700°-1000°C, table 3) there are regions between experimental points where many reactions exist and for which there are no data.

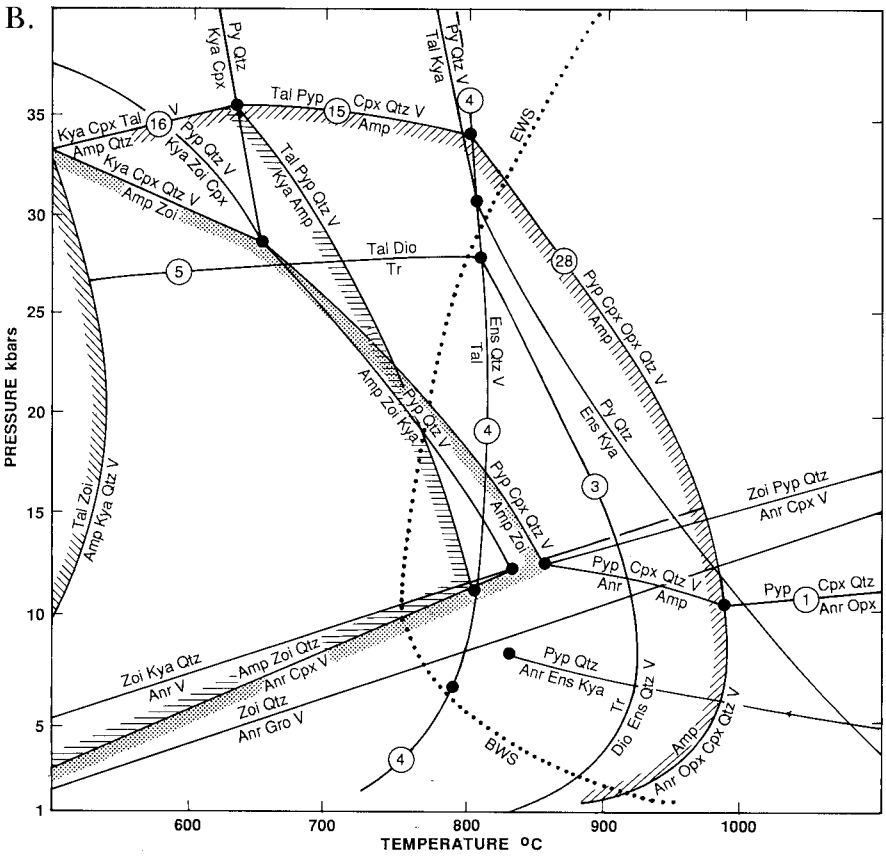

Fig. A-1B

In the text and in some figures (fig. 5) we have considered two cases corresponding to these reaction sequences. This treatment appears to be especially important in the vicinity of the H_2O-saturated solidus from about 15 to 25 kb. Case A corresponds to Amp + Kya reacting out at slightly lower P-T than Zoi + Amp. Case B is the reverse. As emphasized in the text, Sekine, Wyllie, and Baker (1981) have suggested that case A may be appropriate for the simple system CMASH, whereas case B may be relevant to mafic rock compositions.

Just as a final note to colleagues who may wish to use our experiments to refine thermodynamic data bases, it should be said that figure A-1C reproduces extrapolation of our results into the melt-absent (metastable) region, reasonably well. However, most problematical is the implied reaction

$$H_2O + ky + di = zo + py_{90} + qtz \qquad (A2\text{-}1)$$

which according to the calculations has an almost vertical dP/dT with H_2O as part of the low entropy assemblage! This reaction is shown schematically in the boxed region in the upper

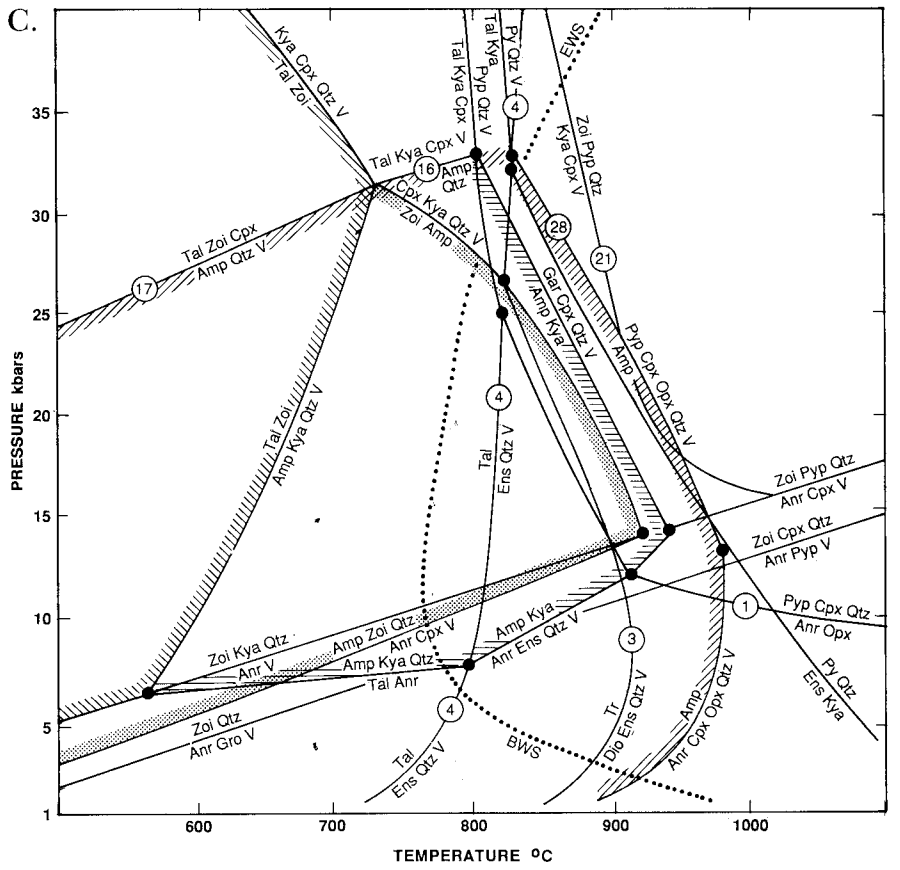

Fig. A-1C

right of figure 7. Strangely enough, such a reaction as (A2-1) could explain the results of the experiments Z-33, Z-30, T-19, T-22 (table 3). We emphasize that such a reaction as (A2-1) may not necessarily be consistent with the results of T.H. Green (1967) who found kyA + cpx stable to 1200°C with up to 4 wt percent H_2O added to basalt, kyanite eclogite, and grosspydite.

References

Abbott, R. N. Jr., 1982, A petrogenetic grid for medium and high grade metabasites: American Mineralogist, v. 67, p. 865–876.

Arth, J. G., Barker, F., Peterman, Z. E., and Friedman, I., 1978, Geochemistry of the gabbro-diorite-tonalite-trondhjemite suite of southwest Finland and its implications for the origin of tonalitic and trondhjemitic magmas: Journal of Petrology, v. 19, p. 289–316.

Arth, J. G., and Hansen, G. N., 1972, Quartz diorites derived by partial melting of eclogite or amphibolite at mantle depths: Contributions to Mineralogy and Petrology, v. 37, p. 161–174.

Beard, J. S., and Lofgren, G. E., 1991, Dehydration melting and water-saturated melting of basaltic and andesitic greenstones and amphibolites at 1, 3 and 6.9 kb: Journal of Petrology, v. 32, p. 365–401.

Berman, R. G., 1988. Internally consistent thermodynamic data for minerals in the system Na_2O-K_2O-CaO-MgO-FeO-Fe_2O_3-Al_2O_3-SiO_2-TiO_2-H_2O-CO_2: Journal of Petrology, v. 29, p. 445–522.

———— 1990, Mixing properties of Ca-Mg-Fe-Mn garnets: American Mineralogist, v. 75, p. 328–344.

Boettcher, A. L., 1970, The system CaO-Al_2O_3-SiO_2-H_2O at high pressures and temperatures: Journal of Petrology, v. 11, p. 337–79.

Boettcher, A. L., and Wyllie, P. J., 1968, Melting of granite with excess water to 30 kilobars pressure: Journal of Geology, v. 76, p. 235–244.

Boyd, F. R., 1959, Hydrothermal investigations of amphiboles, *in* Abelson, P. H., editors, Researches in Geochemistry: New York, John Wiley & Sons, p. 377–96.

Burnham, C. W., 1979a, Magmas and hydrothermal fluids, pp. 71–136, *in* Barnes, H. L., editor, Geochemistry of hydrothermal ore deposits: 2nd edition: New York, Wiley, 798 p.

———— 1979b, The importance of volatile constituents, *in* Yoder, H. S., Jr. editor, The Evolution of the Igneous Rocks: Fiftieth Anniversary Perspectives: Princeton University Press, p. 439–482.

Carroll, M. R., and Wyllie, P. J., 1989, Experimental phase relations in the system tonalite-peridotite-H_2O at 15 kb; implications for assimilation and differentiation processes near the crust-mantle boundary: Journal of Petrology, v. 30, p. 1351–1382.

Cawthorn, R. G., and Brown, P. A., 1976, A model for the formation and crystallisation of corundum-normative calc-alkaline magmas through amphibole fractionation: Journal of Geology, v. 84, p. 467–76.

Cawthorn, R. G., and O'Hara, M. J., 1976, Amphibole fractionation and calc-alkaline magma genesis: American Journal of Science, v. 276, p. 309–29.

Champion, D. C., and Chappell, B. W., 1992, Petrogenesis of felsic I-type granites: an example from northern Queensland: Transactions of the Royal Society of Edinburgh, Earth Sciences, v. 83, p. 115–126.

Chappell, B. W., and Stephens, W. E., 1988, Origin of infracrustal (I-type) granite magmas: Transactions of the Royal Society of Edinburgh, Earth Sciences, v. 79, p. 71–86.

Chinner, G. A., and Dixon, J. E., 1973, Some high pressure parageneses of the Allalin gabbro, Valais, Switzerland: Journal of Petrology, v. 14, p. 185–202.

Chinner, G. A., and Schairer, J. F., 1962, The join $Ca_3Al_2Si_3O_{12}$-$Mg_3Al_2Si_3O_{12}$ and its bearing on the system CaO-MgO-Al_2O_3-SiO_2 at atmospheric pressure: American Journal Science, v. 260, p. 611–34.

Cho, M., and Ernst, W. G., 1991, An experimental determination of calcic amphibole solid solution along the join tremolite-tschermakite: American Mineralogist, v. 76, p. 985–1001.

Clemens, J. D., 1990, The granulite-granite connection, *in* Vielzeuf, D., and Vidal, Ph., editors, Granulites and crustal evolution: Netherlands, Kluwer Academic Publishers, p. 25–36.

Connolly, J. A. D., 1990, Calculation of multivariable phase diagrams: an algorithm based on generalized thermodynamics: American Journal of Science, v. 290, p. 666–718.

Conrad, W. K., Nicholls, I. A., and Wall, V. J., 1988, Water-saturated and undersaturated melting of metaluminous and peraluminous crustal compositions at 10 kb; evidence for the origin of silicic magmas in the Taupo volcanic zone, New Zealand, and other occurrences: Journal of Petrology, v. 29, p. 765–803.

Delaney, J. M., and Helgeson, H. C., 1978, Calculation of the thermodynamic consequences of dehydration in subducting oceanic crust to 100 kb and >800°C: American Journal of Science, v. 278, p. 638–86.

Drummond, M. J., and Defant, M. S., 1990, A model for trondjemite-tonalite-dacite genesis and crustal growth via slab melting: Archean to modern comparisons: Journal of Geophysical Research, v. 95, p. 21503–21521.

Eggler, D. H., 1973, Principles of melting of hydrous phases in silicate melt: Carnegie Institution Washington Year Book, v. 72, p. 491–495.

———— 1978, The effect of CO_2 upon partial melting of peridotite in the system Na_2O-CaO-Al_2O_3-MgO-SiO_2 -CO_2 to 35 kb, with an analysis of melting in a peridotite-H_2O-CO_2 system: American Journal of Science, v. 278, p. 305–343.

Ellis, D. J., 1987, Origin and evolution of granulites in normal and thickened crusts: Geology, v. 15, p. 169–170.

———— 1992: Precambrian tectonics and the physicochemical evolution of the continental crust. II. Lithosphere delamination and ensialic orogeny: Precambrian Research, v. 55, p. 507–524.

Ellis, D. J., and Thompson, A. B., 1986, Subsolidus and partial melting reactions in the quartz-excess CaO + MgO + Al_2O_3 + SiO_2 + H_2O system under water-excess and water-deficient conditions to 10 kb: some implications for the origin of peraluminous melts from mafic rocks: Journal of Petrology, v. 27, p. 91–121.

England, P. C., and Thompson, A. B., 1984, Pressure-temperature-time paths of regional metamorphism I. Heat transfer during the evolution of regions of thickened continental crust: Journal of Petrology, v. 25, p. 894–928.

England, P. C., and Thompson, A. B., 1986, Some thermal and tectonic models for crustal melting in collision zones, *in* Coward, M. P., Ries, A. C., editors, Collision tectonics: Geological Society of London, v. 19, p. 83–94.

Essene, E. J., Hensen, B. J., and Green, D. H., 1970, Experimental study of amphibolite and eclogite stability: Physics of the Earth and Planetary Interiors, v. 3, p. 378–384.

Essene, E. J., Wall, V. J., and Shettel, D., 1973, Equilibria in CaO-MgO-SiO_2-H_2O: Transactions of the American Geophysical Union, v. 54, p. 480.

Evans, B. W., 1990, Phase relations of epidote-blueschists: Lithos, v. 25, p. 3–23.

Gilbert, M. C., Helz, R. T., Popp, R. K., and Spear, F. S., 1982, Experimental studies of amphibole stability, *in* Veblen, D. R., and Ribbe, P. H., editors, Amphiboles: Petrology and Experimental Phase Relations, p. 229–353.

Gill, J. B., 1981, Orogenic andesites and plate tectonics: Springer-Verlag, Berlin, 390 p.

Grant, J. A., 1986, Quartz-phlogopite-liquid equilibria and origins of charnockites: American Mineralogist, v. 71, p. 1071–1075.

Green, D. H., 1973, Experimental melting studies on a model upper mantle composition at high pressure under water-saturated and water-undersaturated conditions: Earth and Planetary Science Letters, v. 19, p. 37–53.

Green, D. H., and Ringwood, A. E., 1967b, An experimental investigation of the gabbro to eclogite transition and its petrological implications: Geochimica et Cosmochimica Acta, v. 31, p. 767–833.

Green, T. H., 1967, An experimental investigation of sub-solidus assemblages formed at high pressure in high-alumina basalt, kyanite eclogite and grosspydite compositions: Contributions to Mineralogy and Petrology, v. 16, p. 84–114.

———— 1982, Anatexis of mafic crust and the high pressure crystallisation of andesite, *in* Thorpe, R. S., editor, Andesites, Orogenic andesites and related rocks: Chichester, John Wiley & Sons, p. 489–522.

———— 1992, Experimental phase equilibrium studies of garnet-bearing I-type volcanics and high level-intrusives from Northland, New Zealand: Transactions of the Royal Society of Edinburgh, v. 83, p. 429–438.

Griffin, B. J., 1979, Energy dispersive analysis system calibration and operation with TAS-SUEDS, and advanced interactive data reduction package: University of Tasmania, Dept. of Geology Publication, 44 p.

Halliday, A. N., Davidson, J. P., Hildreth, W., and Holden, P., 1991, Modelling the petrogenesis of high Rb/Sr magmas: Chemical Geology, v. 92, p. 107–114.

Hammarstrom, J., and Zen, E-an, 1986, Aluminium in hornblende: An empirical igneous geobarometer: American Mineralogist, v. 71, p. 1297–1313.

Hansen, B., 1981, The transition from pyroxene granulite facies to garnet clinopyroxene granulite facies. Experiments in the system CaO-MgO-Al_2O_3-SiO_2: Contributions to Mineralogy and Petrology, v. 76, p. 234–42.

Harley, S. L., and Carswell, D. A., 1990, Experimental studies on the stability of eclogite facies mineral parageneses, *in* Carswell, D. A., editor, Eclogite Facies Rocks: Blackie, Glasgow, p. 52–82.

Helz, R. T., 1976, Phase relations of basalts in their melting ranges at P_{H_2O} = 5 kb. Part II. Melt compositions: Journal of Petrology, v. 17, p. 139–93.

Hensen, B. J., 1976, The stability of pyrope-grossular garnet with excess silica: Contributions to Mineralogy and Petrology, v. 55, p. 279–92.

Holland, T. J. B., and Powell, R., 1990, An enlarged and updated internally consistent thermodynamic dataset with uncertainties and correlations: the system K_2O-Na_2O-CaO-MgO-MnO-FeO-Fe_2O_3 -Al_2O_3-TiO_2-C-H_2-O_2: Journal of Metamorphic Geology, v. 8, p. 89–124.

Hollister, L. S., 1982, Metamorphic evidence for rapid (2 mm/yr) uplift of a portion of the Central Gneiss Complex, Coast Mountains, B.C.: Canadian Mineralogist, v. 20, p. 319–322.

Humphries, D. J., Biggar, G. M., and O'Hara, M. J., 1972, Flow sheet for CaO-MgO-Al_2O_3-SiO_2 at atmospheric pressure: Progress in Experimental Petrology, N.E.R.C. London, U.K., v. 2, p. 138–139.

Irvine, T. N., and Sharpe, M. R., 1982, Source-rock compositions and depths of origin of Bushveld and Stillwater magmas. Yearbook, v. 81, p. 294–302.

Jenkins, D. M., 1981, Experimental phase relations of hydrous peridotites modelled in the system H_2O-CaO-MgO-Al_2O_3-SiO_2: Contributions to Mineralogy and Petrology, v. 77, p. 166–176.

———— 1983, Stability and composition relations of calcic amphiboles in ultramafic rocks: Contributions to Mineralogy and Petrology, v. 83, p. 375–384.

———— 1987, Synthesis and characterisation of tremolite in the system H_2O-CaO-MgO-SiO_2: American Mineralogist, v. 7, p. 707–715.

———— 1988, An experimental study of the join tremolite-tschermakite: A reinvestigation: Contributions to Mineralogy and Petrology, v. 99, p. 392–400.

Jenkins, D. M., Holland, T. J. B., and Clare, A. K., 1991, Experimental determination of the pressure-temperature stability field and thermochemical properties of synthetic tremolite: American Mineralogist, v. 76, p. 458–469.

Jenkins, D. M., Newton, R. C., and Goldsmith, J. R., 1983, Fe-free clinozoisite stability relative to zoisite: Nature, v. 304, p. 622–633.

Johannes, W., Bell, P. M., Mao, H. H., Boettcher, A. L., Chipman, D. W., Hays, J. F., Newton, R. C., and Seifert, F., 1971, An interlaboratory comparison of piston-cylinder pressure calibration using the albite breakdown reaction: Contributions to Mineralogy and Petrology, v. 32, p. 24–38.

Kesson, S. E., and Ringwood, A. E., 1989, Slab-mantle interactions 2. The formation of diamonds: Chemical Geology, v. 78, p. 97–118.

Kitahara, S., Takenouchi, S., and Kennedy, G. C., 1966, Phase relations in the system MgO-SiO_2-H_2O at high temperatures and pressures: American Journal of Science, v. 264, p. 223–233.

Kushiro, I., 1964, The system diopside-forsterite-enstatite at 20 kbars: Carnegie Institution Washington Yearbook, v. 63, p. 101–108.

———— 1969, The system forsterite-diopside-silica with and without water at high pressures: American Journal of Science, v. 267-A, p. 269–294.

Kushiro, I., and Yoder, H. S., 1966, Anorthite-forsterite and anorthite-enstatite reactions and their bearing on the basalt-eclogite transformation: Journal of Petrology, v. 7, p. 337–362.

Lambert, I. B., and Wyllie, P. J., 1972, Melting of gabbro (quartz eclogite) with excess water to 35 kilobars, with geological applications: Journal of Geology, v. 80, p. 693–708.

Léger, A., and Ferry, J. M., 1991, Highly aluminous hornblende from low-pressure metacarbonates and a preliminary thermodynamic model for the Al content of calcic amphibole: American Mineralogist, v. 76, p. 1002–1017.

Lieberman, J. E., and Kamber, B., 1991, Consistent thermodynamic properties for tschermakite from experimental and empirical constraints: EOS, Transactions of American Geophysical Union, v. 72, 564 p.

Liu, T-C., and Presnall, D. C., 1990, Liquidus phase relations on the join anorthite-forsterite-quartz at 20 kbar with applications to basalt petrogenesis and igneous sapphirine: Contributions to Mineralogy and Petrology, v. 104, p. 735–742.

Måder, U. K., and Berman, R. G., 1992, Amphibole thermobarometry: a thermodynamic approach: Geological Society of Canada, Paper 92-1E, p. 393–400.

Mahood, G. A., and Halliday, A. N., 1988, Generation of a high-silica rhyolite: a Nd, Sr and O isotopic study of Sierra La Primavera, Mexican Neovolcanic Belt: Contributions to Mineralogy and Petrology, v. 100, p. 183–191.

Nicholls, I. A., 1974, A direct fusion method of preparing silicate rock glasses for energy-dispersive electron microprobe analysis: Chemical Geology, v. 14, p. 151–157.

Oba, T., 1978, Phase relationships of $Ca_2Mg_3Al_2Si_6O_{22}(OH)_2$-$Ca_2Mg_3Fe^{3+}{}_2Si_6Al_2O_{22}(OH)_2$ join at high temperature and high pressure—the stability of tschermakite: Hokkaido University, Journal of the Faculty of Sciences, Ser. IV, v. 18, p. 339–50.

Obata, M., and Thompson, A. B., 1981, Amphibole and chlorite in mafic and ultramafic rocks in the lower crust and upper mantle: Contributions to Mineralogy and Petrology, v. 77, p. 74–81.

O'Hara, M. J., 1965, Primary magmas and the origin of basalts: Scottish Journal of Geology, v. 1, p. 19–40.

———— 1968, The bearing of phase equilibria studies in synthetic and natural systems on the origin and evolution of basic and ultrabasic rocks: Earth Science Review, v. 4, p. 69–133.

Peacock, S. M., 1990, Fluid processes in subduction zones: Science, v. 248, p. 329–337.

———— 1991, Numerical simulation of subduction zone pressure-temperature-time paths: Constraints on fluid production and arc magmatism: Philosophical Transactions of the Royal Society of London, Ser. A.335, p. 341–353.

Peacock, S. M., Rushmer, T. A., and Thompson, A. B., 1994, Partial melting of subducting oceanic crust: Earth and Planetary Science Letters, v. 121, p. 227–244.

Perkins, III D., 1983, The stability of Mg-rich garnet in the system CaO-MgO-Al_2O_3-SiO_2 at 1000–1300°C and high pressure: American Mineralogist, v. 68, p. 355–364.

Poli, S., 1993, The amphibolite-eclogite transformation: An experimental study on basalt: American Journal of Science, v. 293, p. 1061–1077.

Poli, S., and Schmidt, M. W., 1993, A high pressure study of lawsonite stability in CASH, in basaltic, and in tonalitic systems: Terra abstracts, Abstract supplement 1, Terra nova, v. 5, p. 407.

Rapp, R. P., Watson, E. B., and Miller, C. F., 1991, Partial melting of amphibolite/eclogite and the origin of Archean trondhjemites and tonalites: Precambrian Research, v. 51, p. 1–25.

Richardson, S. W., Gilbert, M. C., and Bell, P. M., 1969, Experimental determination of kyanite-andalusite and andalusite-sillimanite equilibria: the aluminium silicate triple point: American Mineralogist, v. 267, p. 259–272.

Ringwood, A. E., and Green, D. H., 1966, An experimental investigation of the gabbro-eclogite transformation and some geophysical implications: Tectonophysics, v. 39, p. 383–427.

Rushmer, T. A., 1991, Partial melting of two amphibolites: contrasting experimental results under fluid-absent conditions: Contributions to Mineralogy and Petrology, v. 107, p. 41–59.

Schmidt, M. W., 1993, Phase relations and compositions in tonalite as a function of pressure: An experimental study at 650°C: American Journal of Science, v. 293, p. 1011–1060.

Schmidt, M. W., and Thompson, A. B., 1993, Epidote in Tonalite. Terra Abstracts, Abstract supplement 1, Terra nova, v. 5, p. 563.

Schreyer, W., 1988, Experimental studies on metamorphism of crustal rocks at mantle pressures: Mineralogical Magazine, v. 52, p. 1–26.

Sekine, T., Wyllie, P. J., and Baker, D. R., 1981, Phase relationships at 30 kbar for quartz eclogite composition in CaO-MgO-Al_2O_3-SiO_2-H_2O with implications for subduction zone magmas: American Mineralogist, v. 66, p. 938–950.

Stern, C. R., and Wyllie, P. J., 1978, Phase compositions through crystallization intervals in basalt-andesite-H_2O at 30 kbar with implications for subduction zone magmas: American Mineralogist, v. 63, p. 641–663.

Stewart, D. B., 1967, Four-phase curve in the system $CaAl_2Si_2O_8$-SiO_2-H_2O between 1 and 10 kilobars: Schweizerische mineralogisch-petrographische Mitteilungen, v. 47, p. 35–59.

Thompson, A. B., 1982, Dehydration melting of pelitic rocks and the generation of H_2O-undersaturated granitic liquids: American Journal of Science, v. 282, p. 1567–1595.

———— 1990, Heat, fluids, and melting in the granulite facies, *in* Vielzeuf, D., and Vidal, Ph., editors, Granulites and Crustal Evolution: NATO ASI Series, 311, Kluwer, Dodrecht, p. 37–57.

———— 1992, Water in the Earth's upper mantle: Nature, v. 358, p. 295–302.

Thompson, J. B., 1981, An introduction to the mineralogy and petrology of biopyriboles, *in* Veblen, D. R., editor, Amphiboles and other hydrous pyriboles—Mineralogy: Mineralogical Society of America, Reviews in Mineralogy, v. 9A, p. 141–188.

———— 1982, Reaction space: an algebraic and geometric approach: Mineralogical Society of America, Reviews in Mineralogy, v. 10, p. 33–52.

Thompson, J. B., Laird, J., and Thompson, A. B., 1982, Reactions in amphibolite, greenschist and blueschist: Journal of Petrology, v. 23, p. 1–27.

Troll, G., and Gilbert, M. C., 1972, Fluorine-hydroxyl substitution in tremolite: American Mineralogist, v. 57, p. 1386–1403.

Vernon, R. H., 1976, Metamorphic Processes: London, Allen and Unwin, 247 p.

Vielzeuf, D., and Clemens, J. D., 1992, The fluid-absent melting of phlogopite + quartz: Experiments and models: American Mineralogist, v. 77, p. 1206–1222.
Warner, R. D., 1975, New experimental data for the system CaO-MgO-SiO_2-H_2O and a synthesis of inferred phase relations: Geochimica et Cosmochimica Acta, v. 39, p. 1413–1421.
Welch, M. A., and Pawley, A. R., 1991, Tremolite: New enthalpy and entropy data: American Mineralogist, v. 76, p. 1931–1939.
Wickham, S. M., and Oxburgh, E. R., 1988, Evolution of the lower crust: Nature, v. 333, p. 119–120.
White, A. J. R., and Chappell, B. W., 1977, Ultrametamorphism and granitoid genesis: Tectonophysics, v. 43, p. 7–22.
Wones, D. R., and Dodge, F. C. W., 1977, The stability of phlogopite in the presence of quartz and diopside, *in* Fraser, D. G., editor, Thermodynamics in Geology: Dordrecht, Reidel, p. 229–247.
Wood, B. J., 1987, Thermodynamics of multicomponent systems containing several solid solutions, *in* Carmichael, I. S. E., and Eugster, H. P., editors, Thermodynamic modelling of geological materials: minerals, fluids and melts: Mineralogical Society of America, Reviews in Mineralogy, v. 17, p. 71–96.
Yoder, H. S., and Kushiro, I., 1969, Melting of a hydrous phase, Phlogopite: American Journal of Science, v. 267-A, p. 558–582.
Yoder, H. S., and Tilley, C. E., 1962, Origin of basaltic magmas: an experimental study of natural and synthetic rock system: Journal of Petrology, v. 3, p. 342–532.
Zen, E-an, 1985, Implications of magmatic epidote-bearing plutons on crustal evolution in the accreted terranes of northwestern North America: Geology, v. 13, p. 266–269.[8]